NACA RM A55D27

RESEARCH MEMORANDUM

EXPERIMENTAL INVESTIGATION AT MACH NUMBERS FROM 0 TO 1.9 OF TRAPEZOIDAL AND CIRCULAR SIDE INLETS FOR A FIGHTER-TYPE AIRPLANE

By Emmet A. Mossman, Frank A. Pfyl,
and Frank A. Lazzeroni

Ames Aeronautical Laboratory
Moffett Field, Calif.

NATIONAL ADVISORY COMMITTEE
FOR AERONAUTICS

WASHINGTON
July 28, 1955

NATIONAL ADVISORY COMMITTEE FOR AERONAUTICS

RESEARCH MEMORANDUM

EXPERIMENTAL INVESTIGATION AT MACH NUMBERS FROM 0 TO 1.9 OF TRAPEZOIDAL AND CIRCULAR SIDE INLETS FOR A FIGHTER-TYPE AIRPLANE

By Emmet A. Mossman, Frank A. Pfyl,
and Frank A. Lazzeroni

SUMMARY

An experimental investigation was conducted to determine the performance characteristics of two side inlets of dissimilar shape. One of the inlets was approximately trapezoidal in cross section and the other was circular. The trapezoidal inlet was investigated with both blunt and thin lips and, for both arrangements, was fitted with a 7° compression ramp. No external compression surface was used with the circular inlet which was investigated with only one lip contour. Tests were made at Mach numbers from 0 to 1.9, angles of attack from 0° to 10°, and mass-flow ratios from 0 to the maximum obtainable.

Of the inlets tested at supersonic speeds, the circular inlet had the lowest drag, the highest net-propulsive thrust, and the largest stable range of operation. The advantage of the circular inlet over the trapezoidal inlets, from a drag standpoint, was shown to be associated with the type of boundary-layer removal system, the reduced angularity of the external contours in the vicinity of the inlet entrance, and a smaller projected frontal area.

For each of the inlets investigated, when the magnitude of the pressure pulsations started to increase, a flow asymmetry occurred in which one side of the air-induction system operated at a higher mass-flow ratio than the other side.

Performance analysis for each of the inlets on the basis of a net-thrust parameter showed that a fixed inlet area could be used satisfactorily at Mach numbers up to 1.5. However, the circular inlet showed more favorable off-design operation, except at take-off.

INTRODUCTION

The performance of side-scoop air-induction systems is dependent, in part, on the magnitude of the losses resulting from the interaction of the boundary layer in front of the inlet with the shock waves accompanying the supersonic compression. Since side inlets normally are placed in the proximity of the thick viscous boundary layer of the fuselage, it has proven advantageous to move the compression surfaces out from the fuselage a distance about equal to the thickness of the boundary layer. This method of bleeding off the low-energy fuselage boundary layer before it reaches the inlet has met with some degree of success (refs. 1 to 3), but side inlets utilizing boundary-layer control have not attained the performance of nose inlets of similar designs. In addition, the systems used for diverting or removing the fuselage boundary layer from in front of the inlet may add a considerable drag penalty which is chargeable to the inlets.

In the present study, two inlet types, one trapezoidal and the other circular in shape, were investigated. The trapezoidal inlets were, in general, similar to other side-inlet designs having compression ramps in front of the entrance. About 30 percent of the entrance perimeter of the trapezoidal inlets is adjacent to the fuselage boundary layer. The pressure drag on the wedge faces, the friction drag on the surrounding surfaces, and the mixing losses involved in directing the bleed flow downstream of the inlet contributes substantial drag penalties on side-inlet air-induction systems. In order to minimize the interference and mixing losses to the flow near the fuselage as it is directed around the air-induction system, circular side inlets were designed. A similar circular scoop inlet has been investigated and is reported in references 4 and 5. In these studies the scoop inlet was located forward on the fuselage near the apex of the nose where the fuselage boundary layer is thin. With circular inlets located one boundary-layer height away from the fuselage, the entrance perimeter has only point contact with the thick viscous boundary layer. The mixing losses of the boundary-layer flow around the circular inlet are believed to be less than those for the trapezoidal inlets. It is believed that reductions in the mixing losses can occur if the boundary layer beneath the inlet is not confined in a narrow passage. Also, somewhat lower pressure drag of the circular-inlet boundary-layer bleed surfaces would be expected since, in the present application, the wedge diverter has a lower equivalent angle.

Because of the unknown mixing and viscous forces, and the distortion of the flow field into which the inlets are placed, it is not possible to predict theoretically which of the two inlets would result in the best propulsive effort. Accordingly, an experimental investigation was made to compare the drag, pressure recovery, and mass-flow characteristics of the trapezoidal and circular side inlets. The performances of the inlets are compared analytically by means of a net-thrust parameter.

[redacted]

The results of the experimental investigation are presented herein for Mach numbers of 0, 0.9, 1.3, 1.5, 1.7, and 1.9 at a constant tunnel stagnation pressure of 10 pounds per square inch absolute.

NOTATION

A	area, sq ft
C_D	net drag coefficient, $\frac{D}{qS}$
D	net drag, lb (measured drag minus internal drag)
M	Mach number
m	mass flow through inlet (measured at compressor station), slugs/sec
$\frac{m}{m_\infty}$	ratio of the mass flow through the inlet to the mass flow at the free-stream conditions passing through an area equal to the inlet entrance area $\frac{\rho_c A_c V_c}{\rho_\infty A_i V_\infty}$
N.S.	normal-shock pressure recovery
p	static pressure, lb/sq ft
p_t	total pressure, lb/sq ft
$\frac{p_{t_c}}{p_{t_\infty}}$	total-pressure ratio at the compressor station
q	dynamic pressure, lb/sq ft
R	Reynolds number
S	wing area, 8.703 sq ft
T_I	net thrust with isentropic pressure recovery, lb
T_N	net thrust with measured pressure recovery, lb
V	velocity, ft/sec
$\frac{W_a\sqrt{\theta}}{A_i\delta}$	air-flow parameter, lb/sec ft^2

[redacted]

W_a air-flow rate, lb/sec

α angle of attack of fuselage reference axis, deg

δ compressor station total pressure divided by NACA sea-level static pressure

η net-thrust parameter, $\frac{T_N - D}{T_I}$

θ absolute total temperature divided by absolute NACA ambient sea-level temperature

ρ mass density of air, slugs/cu ft

Subscripts

c compressor station

i inlet entrance station

∞ free-stream condition

APPARATUS AND PROCEDURE

The partial model of the fighter-type airplane used in the tests was sting mounted in the Ames 6- by 6-foot supersonic wind tunnel. One of the two inlets used in conjunction with the model had an approximate trapezoidal cross-sectional area, and the other was of circular cross section. A blunt lip and a thin lip were tested with the trapezoidal-shaped inlet, but only one relatively sharp lip was used with the circular inlet. Two body cross-sectional areas were tested with the circular inlet. These inlets are referred to in the remainder of this report as the blunt-lip inlet, the thin-lip inlet, the circular inlet, and the circular inlet plus area. Photographs of the model with the blunt-lip inlet and the circular inlet, showing the approximate trapezoidal and circular shapes, respectively, are presented in figures 1 and 2. A comparison of the inlet region for the three inlet configurations can be seen in the photograph of figure 3. The blunt- and thin-lip inlets had 7° compression surfaces ahead of the inlet but the circular inlet had no external compression surface. All inlets had a negative incidence of 4° relative to the fuselage reference plane. The inlets were designed for operation at Mach numbers from 0 to 1.5.

[redacted]

The differences in the longitudinal area distribution of the air-induction model with each of the inlets (fig. 4) were kept small. Lip coordinates are given in figure 5. The variation of the diffuser internal area for each inlet shape is shown in figure 6. A schematic comparison of the fuselage boundary-layer diverter wedges for the three inlets is given in figure 7.

Figure 8 is a sketch showing the location and number of tubes of the total- and static-pressure tubes at the simulated compressor inlet, and the position of the pressure cells for measuring air-flow instability. The mass flow through the model obtained from total- and static-pressure measurements at the compressor inlet was calibrated against an A.S.M.E. orifice meter prior to the wind-tunnel tests. The calibration factor from these bench tests and the integrated total and static pressures were used in obtaining the mass flow through the model during the wind-tunnel investigation. The quantity of air flow through the duct was regulated by a movable plug at the exit of the model (see fig.8). The pressure cells used in the investigation were of the strain-gage type which have response invariant with frequency from 0 to 10,000 cycles per second. However, the carrier current amplifier and recording oscillograph apparatus reduce this linear frequency range from 0 to 10,000 cycles per second to approximately 0 to 500 cycles per second for the over-all instrumentation. Values of the maximum total amplitude of the pressure pulsations were obtained from pressure-time records of the strain-gage pressure cell mounted in the duct system.

Reference 6 indicates that the boundary layer on bodies of revolution tested at the Reynolds numbers of this investigation could be in a transitional range. To insure that the frictional forces would remain relatively constant, transition was fixed on the nose of the body (two 0.01-inch-diameter wires 1/2 inch apart, the first wire 1 inch from the tip) and near the leading edge of the lip of the inlet (one 0.01-inch-diameter wire, 1/2 inch from the leading edge of the lip). The drag increment between each configuration is unaffected by the presence of the transition wires since the wires were installed identically on each configuration.

A six-component strain-gage balance inside the model was used to measure the forces. In the reduction of data, the forces developed by the internal flow and the base forces were subtracted from the balance measured values. The internal force is defined as the change in total momentum of the entering stream tube from the free stream to the exit of the model, and is thus consistent with the usual definition of jet-engine thrust. The total momentum of the stream tube at the exit of the model was calculated by using the corrected mass flow through the duct and the area-weighted average total pressure at the rake station.

Tests were made for a range of mass-flow ratios from 0 to the maximum obtainable, angles of attack up to 10°, and Mach numbers of 0, 0.9, 1.3, 1.5, 1.7, and 1.9. Drag data are not presented at $M_{\infty} = 1.3$ because the

[redacted]

reflection of the bow shock wave from the tunnel wall intersected the afterportion of the model. Except for the static tests ($M_\infty = 0$) and $M_\infty = 1.3$, all experiments were made with a constant tunnel stagnation pressure of 10 pounds per square inch absolute. The Reynolds number per foot is given in the following table.

Mach number	Reynolds number per foot, million
0.9	3.0
1.3	2.5
1.5	2.9
1.7	2.8
1.9	2.6

RESULTS

The pressure recovery for the simulated take-off ($M_\infty = 0$) is given in figure 9 for the three inlets. Comparisons of the pressure recovery and drag for the blunt-lip inlet, the thin-lip inlet, and the circular inlet are presented in figure 10 for Mach numbers of 0.9, 1.3, 1.5, 1.7, and 1.9 at an angle of attack of 4°. Angle-of-attack performance, which was obtained only for the blunt-lip inlet and the circular inlet, is given in figures 11 and 12 for Mach numbers of 0.9 and 1.5. Schlieren photographs at $\alpha = 4^\circ$ and $M_\infty = 1.5$ (fig. 13) show the shock-wave patterns characteristic of each of the three inlet configurations. A typical pressure-time record for one of the strain-gage pressure cells is shown in figure 14. From such records the maximum total amplitude of the pressure pulsations in the duct was determined for each test point, these points being recorded on figure 15 for the three inlet configurations. Representative contour maps of the total-pressure recovery at the compressor station are shown in figure 16 for each inlet at $M_\infty = 1.5$ for a mass-flow ratio of approximately 0.90 and $\alpha = 4^\circ$.

DISCUSSION

Pressure Recovery

A survey of the literature on normal-shock inlets (refs. 7 to 12) indicated that a normal-shock scoop-inlet installation might prove satisfactory for speeds up to a Mach number of 1.5, although the pressure recovery of the scoop-type inlets is, generally, lower than for nose inlets. It was found in this investigation, however, that the circular inlet gave nearly equal or somewhat higher recoveries than the nose inlets of references 8 and 12.

[redacted]

At Mach numbers of 0.9 and 1.3, the pressure recovery of the circular inlet was not significantly different from the blunt-lip and thin-lip inlets. At higher Mach numbers, the ramp-type inlets tested had higher pressure recoveries at mass-flow ratios greater than about 0.8 (see fig. 10). It should be noted, however, that installation of a compression surface in the circular inlet could increase the pressure recovery at the higher mass-flow ratios at Mach numbers above about 1.5. The increase in pressure recovery above that for a normal shock, shown for the circular inlet at mass-flow ratios below 0.8, appeared in the schlieren photographs of figure 13(c) to be caused by an oblique shock formation in front of the inlet and the fact that the separated boundary layer did not enter the inlet.

There was very little difference in the pressure recovery between the blunt-lip and thin-lip inlets over the major portion of the mass-flow range. However, the blunt-lip inlet, generally, had slightly higher values of pressure recovery in the region of maximum mass-flow ratio at all Mach numbers, and in the take-off condition ($M_\infty = 0$, fig. 9) it was definitely superior to either the thin-lip or circular inlet.

Figures 11(b) and 12(b) show that the pressure recovery of both the blunt-lip and circular inlets at a Mach number of 1.5 was insensitive to changes in angle of attack (between 0° and 10°). At $M_\infty = 0.9$ and mass-flow ratios greater than about 0.80, the pressure recovery was reduced for angles of attack above 4° with the circular inlet and above 7° with the blunt-lip inlet. For the blunt-lip inlet, at $M_\infty = 0.9$, a discontinuity is evident in the pressure recovery for angles of attack above and below 4° at a mass-flow ratio near 0.55. This sudden reduction in recovery occurred in conjunction with large pressure fluctuations in the duct.

Drag

One of the advantages of the circular inlet over the trapezoidal inlets for this airplane is the decrease in volume of the structure surrounding the duct system, because of the structural superiority of the circular shape. This decrease in internal structure would be reflected in reduced angularity with respect to the free-stream direction of the external contours of the model in the vicinity of the inlet. The longitudinal area distribution for the air-induction model with the various inlet configurations, figure 4, shows that the maximum cross-sectional area of the model with the circular inlet is slightly less than either the blunt- or thin-lip inlets. Experimental tests made with the circular inlet having its maximum cross-sectional area increased to that of the blunt-lip inlet (see figs. 4 and 10), showed that the cross-sectional-area increase accounted for a 0.0004 increment in C_D at supersonic speeds, and had no measurable effect at $M_\infty = 0.9$. Certain existing structural members

however, restricted further changes in angularity of the duct surfaces; thus the maximum drag reduction possible could not be realized on the circular-inlet model.

At $M_\infty = 0.9$ the drag coefficients of the three inlet configurations were about the same (fig. 10(a)). However, the thin-lip inlet and the circular inlet had considerably lower drag coefficients than the blunt-lip inlet at supersonic speeds. The drag difference between the blunt-lip and the thin-lip inlets was about what would be expected from previous research reported in reference 8. The magnitude of the decrease in drag resulting from use of the circular inlet, assuming a total drag coefficient of the airplane in high speed flight ($M_\infty = 1.5$) of 0.0235, would reduce the airplane drag 10 percent over the configuration using the blunt-lip inlet and 5 percent over the thin-lip inlet configuration. This reduction in drag may be partly the result of the previously mentioned external contouring advantages of the circular inlet, but, as mentioned in the Introduction, is believed to be due mainly to the difference in the boundary-layer diverter systems.

The increase in drag with increasing angle of attack (above 4°) is less rapid with the circular inlet than with the blunt-lip inlet at Mach numbers of 0.9 and 1.5 (see figs. 11 and 12.) However, the drag rise between 0° and 4° is small for either inlet at both subsonic and supersonic speeds.

Air-flow Stability

The criterion used to indicate the degree of instability of the inlets tested was the maximum total amplitude of the pressure pulsations measured by the pressure cells in the ducting system. Examination of the pressure-time records showed the pressure pulsations to be random, and to have a maximum frequency of about 450 cycles per second (see fig. 14). These records showed that the start of "buzz" (see fig. 15) was at lower mass-flow ratios and that the maximum amplitude of the pressure pulsations was much less for the circular inlet than for either the blunt- or thin-lip inlets. Although the maximum pressure amplitude in the circular inlet diffuser never exceeded 5 percent of the total pressure, lower oscillation amplitudes over a wider mass-flow range might be expected by increasing the distance between the fuselage and the adjacent circular entrance. A possible explanation for the lower pressure pulsations in the circular inlet may be that the circular inlet allows a major portion of the air separated by shock-wave boundary-layer interaction to pass around the inlet. A somewhat similar argument may be obtained from an investigation of a normal-shock inlet reported in reference 11. When the normal shock was in front of the splitter plate of the modified inlet (ref. 11), a portion of the separated air was removed by the boundary-layer bleed system and the magnitude of the oscillation amplitudes was reduced.

[redacted]

From the records of the pressure pulsations in the duct, and from visual schlieren and manometer-tube observations, it was noted that when the magnitude of the flow instability increased rapidly, a flow asymmetry usually occurred (see fig. 13(a)). The inlet on one side of the model had a larger air flow through it than the inlet on the opposite side, with the result that the buzz was also more severe on the side inlet with the lowest air flow. A similar phenomenon has been observed in other side-inlet installations, both at subsonic (ref. 13) and at supersonic speeds (ref. 14) where the ducting from two inlets join in a common chamber.

At the high subsonic speed of these tests, $M_\infty = 0.9$, and at low mass-flow ratios (m/m_∞ less than about 0.5), instability occurred for the blunt-lip inlet at angles of attach above and below 4°, and for the thin-lip inlet at 4°. Evidence of the instability can be seen both from the increase in the total amplitude of the pressure pulsations (fig. 15(a)) and from the pressure-recovery mass-flow ratio curves of figure 11(a). The instability probably was triggered by separation on the ramp and in some instances resulted in the twin-duct type of instability. For the circular inlets at subsonic speed, no internal flow instability occurred at any of the angles of attack tested (figs. 12(a) and 15).

Total Pressure Distribution

The performance of a jet engine in combination with an air-induction system has been found to be a function of both the average pressure of the air delivered to the engine, and the radial and circumferential pressure distribution of the flow at the entrance to the compressor. Poor distribution can also produce severe vibratory stresses. Representative contour maps showing the pressure variation at the compressor entrance indicate differences in the radial and circumferential total pressures of about ±7.0 percent, at a simulated high-speed condition, ($M_\infty = 1.5$, $m/m_\infty \approx 0.9$). A study of these plots (fig. 16) and of data at other flight conditions indicates the same degree of nonuniformity in radial and peripheral total pressure distribution for the three inlet configurations.

It should be pointed out that at lower mass-flow ratios than those presented in figure 16 the pressure variations in the duct were more uniform, while the distribution at higher mass flow was less uniform.

Net Propulsive Force

A significant performance comparison of the three inlets tested involves a conversion of the drag force and the pressure recovery into a single net-thrust parameter. The inlets must also be compared at their

actual operating points. At the operating (or "matched") condition, the air supplied by the inlet must be equal to the air required by the engine (for this analysis the JT3C-20 engine was assumed). The method used and the assumption involved in this performance analysis are given in reference 8. The only modification to the method outlined in reference 8 is that in the present report a net-thrust parameter is used, while in reference 8 the results were given in terms of an effective drag coefficient. The drag force used in the computations is for the fuselage and air-induction system shown in figures 1 and 2, and does not include the drag of wing or tail surfaces.

The results of the analysis for each of the three inlets investigated are given in figure 17. In general, the circular inlet can be seen to have considerably better net propulsive thrust than either the blunt- or thin-lip trapezoidal inlets. At supersonic speeds, the thin-lip inlet gives a higher net-thrust parameter than the blunt-lip inlet. It should be noted that at supersonic speeds the change in the net-thrust parameter with inlet area (or mass-flow ratio) is much less for the circular inlet than for either the blunt- or thin-lip inlets; indicating a more favorable off-design performance for the circular inlet.

The inlet area of 4.21 square feet appears to be a good compromise when the performace in the speed range from 0 to 1.5 is considered. Somewhat higher performace at supersonic speeds can be attained with an inlet area of 3.5 square feet; however, severe performance losses are incurred during subsonic operation.

It should be remembered that the inlets tested were designed, primarily, for operation at Mach numbers up to 1.5. By designing the inlets for operation at higher Mach numbers the net-thrust parameter would be changed considerably at all speeds.

CONCLUSIONS

The following conclusions were obtained from an investigation at Mach numbers from 0 to 1.9 of a side-inlet air-induction system for a fighter-type airplane:

1. Of the inlets tested at supersonic speeds on the air-induction model, the circular inlet had the lowest drag, highest net propulsive thrust, and largest stable range of operation.

2. The advantage of the circular inlet over the trapezoidal inlets, from a drag standpoint, appeared to be associated with the combined effects of the type of boundary-layer removal system, reduced angularity of the external contours near the lip entrance, and a smaller projected frontal area.

[redacted]

3. For the trapezoidal inlets at supersonic speeds, the thin-lip design had less drag than the blunt-lip design.

4. At $M_\infty = 1.5$ the variation of pressure recovery with angle of attack up to 7° was insignificant for either the blunt-lip, trapezoidal inlet, or the circular inlet.

5. The flow instability encountered with these inlets was accompanied, usually, by a flow asymmetry in which the inlet on one side operated at a higher mass-flow ratio than the inlet on the other side.

6. Analysis of the inlet performance on the basis of a net-thrust parameter showed that a fixed inlet area could be used satisfactorily at Mach numbers up to 1.5. The circular inlet also showed more favorable off-design operation, except at take-off.

Ames Aeronautical Laboratory
National Advisory Committee for Aeronautics
Moffett Field, Calif., Apr. 27, 1955

REFERENCES

1. Valerino, Alfred S.: Performance Characteristics at Mach Numbers to 2.0 of Various Types of Side Inlets Mounted on Fuselage of Proposed Supersonic Airplane. I - Two-Dimensional Compression-Ramp Inlets With Semicircular Cowls. NACA RM E52E02, 1952.

2. Obery, Leonard J., and Stitt, Leonard E.: Investigation at Mach Numbers 1.5 and 1.7 of Twin-Duct Side Air-Intake System with 9° Compression Ramp Including Modifications to Boundary-Layer-Removal Wedges and Effects of a Bypass System. NACA RM E53H04, 1953.

3. Campbell, Robert C., and Kremzier, Emil J.: Performance of Wedge-Type Boundary Layer Diverters for Side Inlets at Supersonic Speeds. NACA RM E54C23, 1954.

4. Merlet, Charles F., and Carter, Howard S.: Total-Pressure Recovery of a Circular Underslung Inlet With Three Different Nose Shapes at a Mach Number of 1.42. NACA RM L51K05, 1952.

5. Merlet, Charles F.: Pressure Recovery and Drag Characteristics of a Forward Located Circular Scoop Inlet as Determined from Flight Tests for Mach Numbers from 0.8 to 1.6. NACA RM L54B23, 1954.

6. Czarnecki, K. R., and Sinclair, Archibald, R.: Factors Affecting Transition at Supersonic Speeds. NACA RM L53118a, 1953.

[redacted]

7. Blackaby, James R.: An Analytical Study of the Comparative Performance of Four Air-Induction Systems for Turbojet-Powered Airplanes Designed to Operate at Mach Numbers up to 1.5. NACA RM A52C14, 1952.

8. Mossman, Emmet A., and Anderson, Warren E.: The Effect of Lip Shape on a Nose-Inlet Installation at Mach Numbers from 0 to 1.5 and a Method for Optimizing Engine-Inlet Combinations. NACA RM A54B08, 1954.

9. Fraser, Alson C., and Anderson, Warren E.: Performance of a Normal-Shock Scoop Inlet With Boundary-Layer Control. NACA RM A53D29, 1953.

10. Dryer, Murray, and Beke, Andrew: Performance Characteristics of a Normal-Shock Side Inlet Located Downstream of a Canard Control Surface at Mach Numbers of 1.5 and 1.8. NACA RM E52F09, 1952.

11. Mossman, Emmet A., Lazzeroni, Frank A., and Pfyl, Frank A.: An Experimental Investigation of the Air-Flow Stability of a Scoop-Type Normal-Shock Inlet. NACA RM A55A13, 1955.

12. Brajnikoff, George B., and Rogers, Arthur W.: Characteristics of Four Nose Inlets as Measured at Mach Numbers between 1.4 and 2.0. NACA RM A51C12, 1951.

13. Martin, Norman J., and Holzhauser, Curt A.: Analysis of Factors Influencing the Stability Characteristics of Symmetrical Twin-Intake Air-Induction Systems. NACA TN 2049, 1950.

14. Davids, Joseph, and Wise, George A.: Investigation at Mach Numbers 1.5 and 1.7 of Twin-Duct Side Intake System With Two-Dimensional 6° Compression Ramps Mounted on a Supersonic Airplane. NACA RM E53H19, 1953.

[redacted]

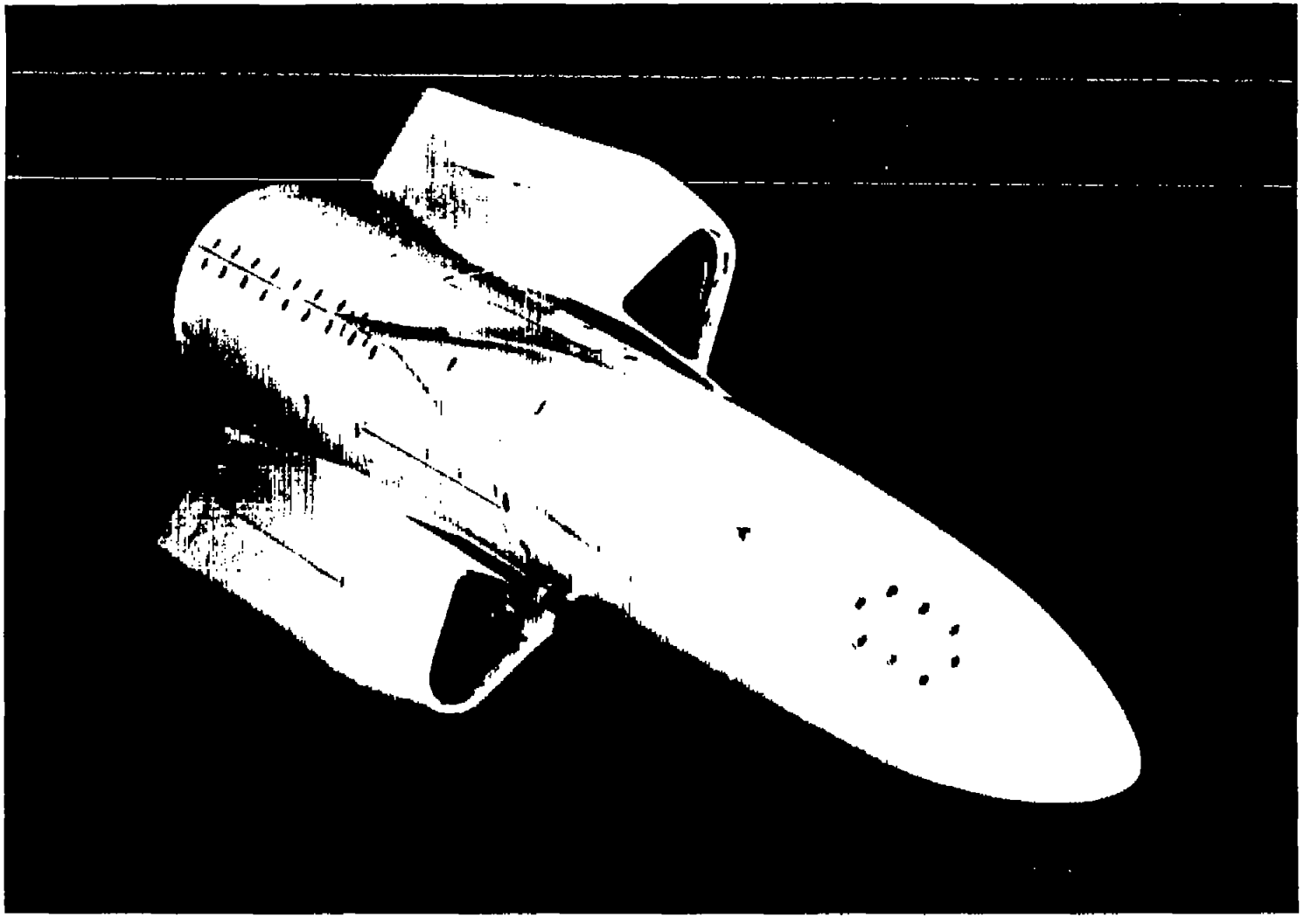

A-19399.1

Figure 1.- Photograph of the air-induction model with the blunt-lip inlet.

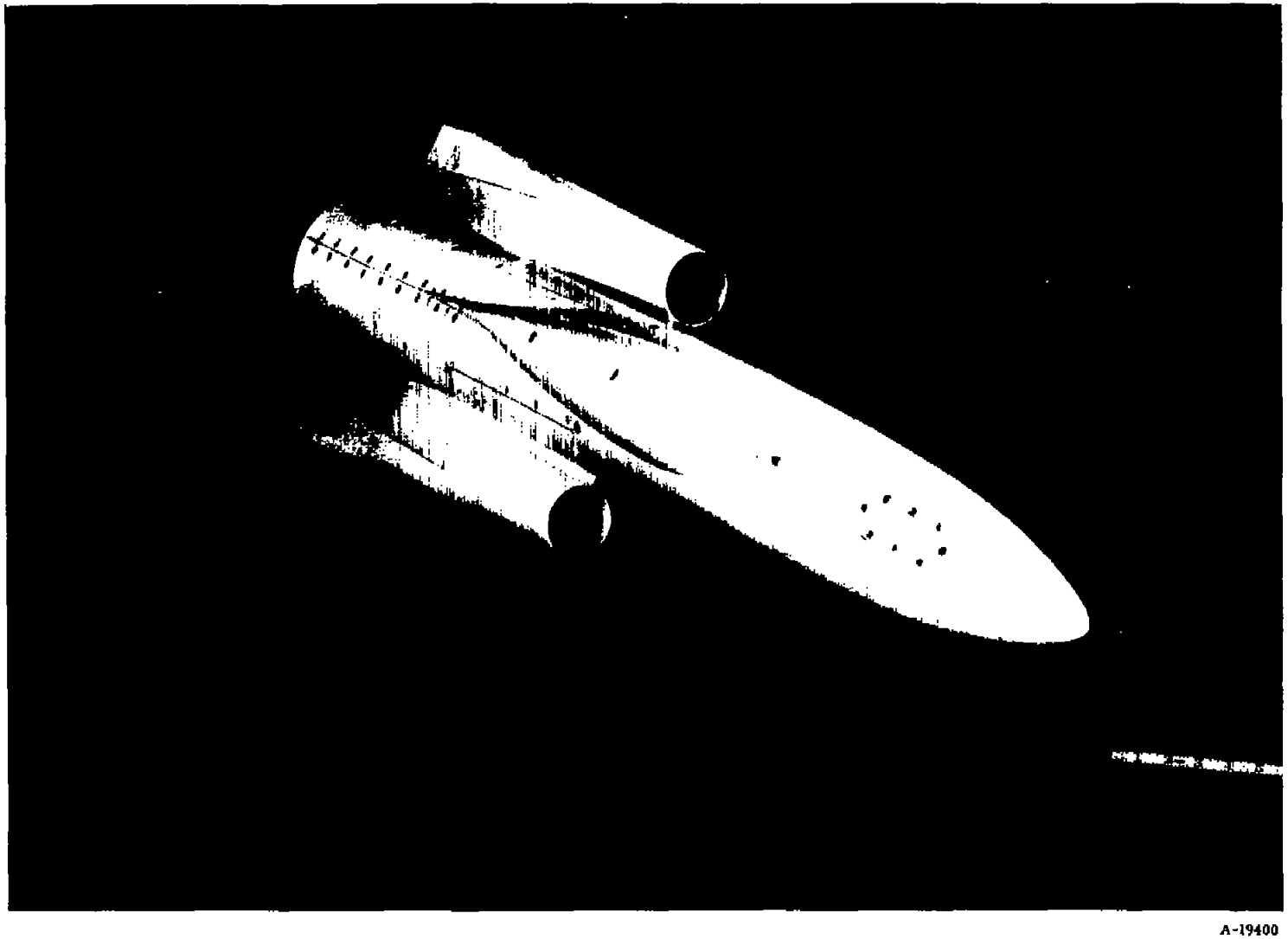

A-19400

Figure 2.- Photograph of the air-induction model with the circular inlet.

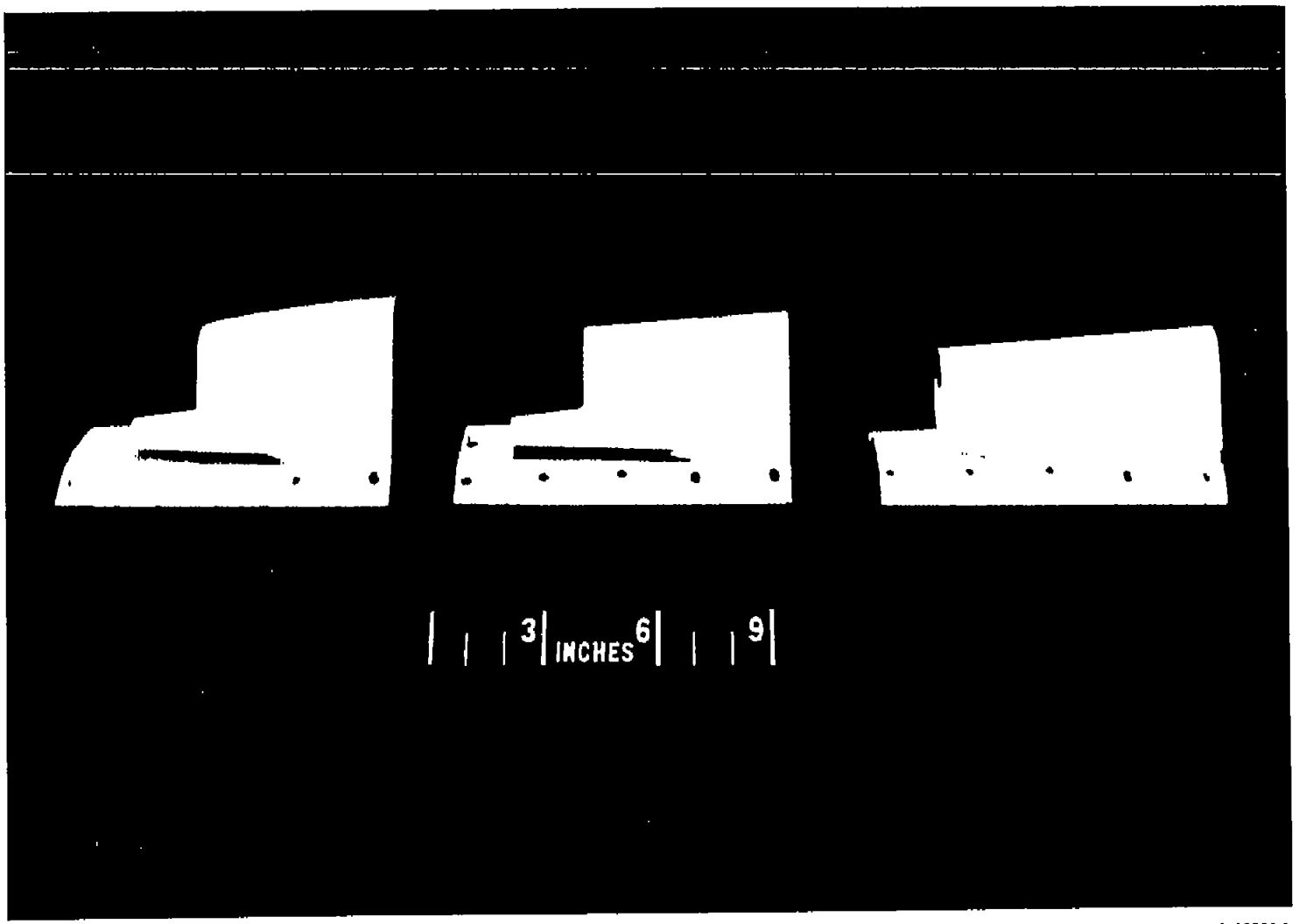

Figure 3.- Photograph showing the inlet region for the blunt-lip, thin-lip, and circular inlets.

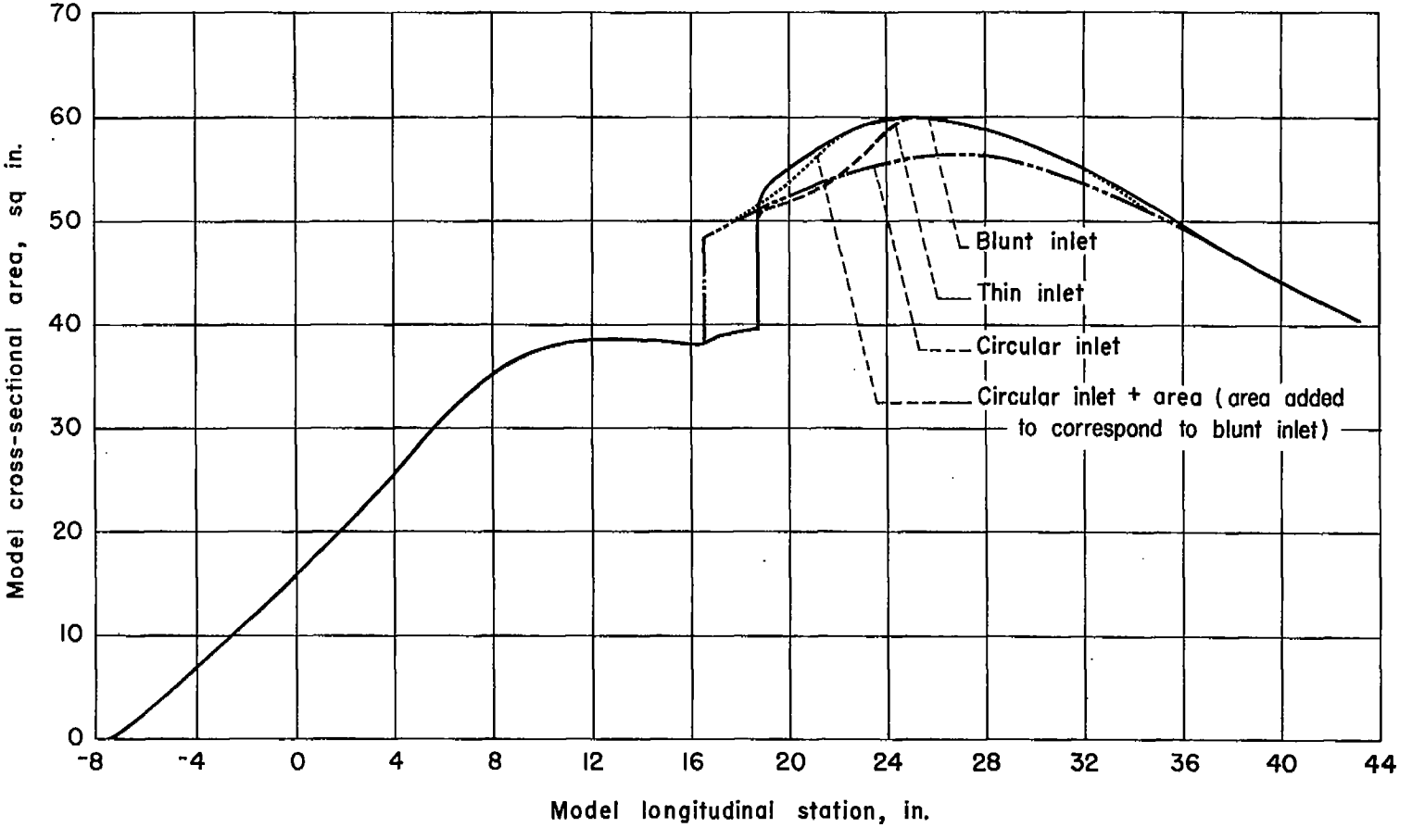

Figure 4.- Area distribution of the air-induction model with the blunt-lip inlet, the thin-lip inlet, and the circular inlet.

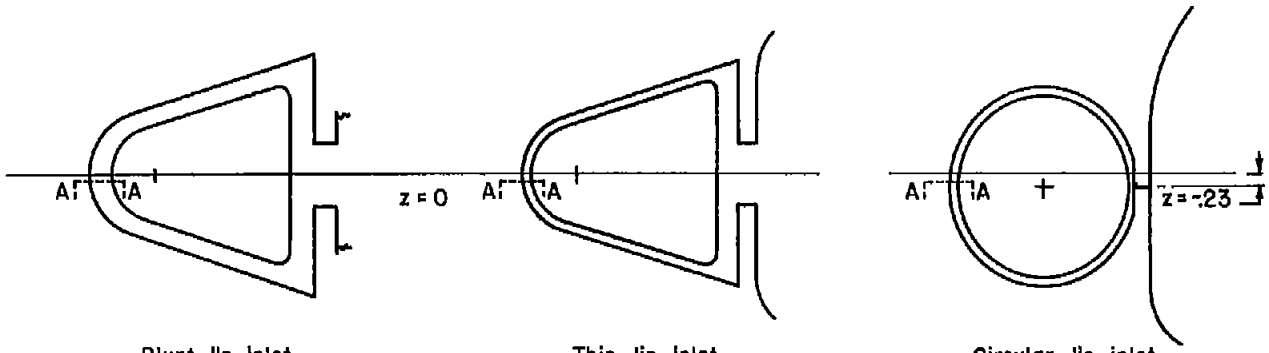

Blunt lip inlet | Thin lip inlet | Circular lip inlet

Leading edge radius = .0625		
x	y_1	y_2
0	0	0
.05	.070	.080
.10	.090	.110
.15	.105	.135
.20	.115	.155
.25	.124	.173
.30	.130	.190

Leading edge radius = .0325		
x	y_1	y_2
0	0	0
.05	.048	.048
.10	.059	.063
.15	.065	.071
.20	.066	.075
.25	.066	.078
.30	.066	.081

Leading edge radius = .0156		
x	y_1	y_2
0	0	0
.005	.013	.012
.0188	.020	.015
.0500	.030	.017
.100	.040	.020
.150	.045	.024
.250	.045	.032
.500	.045	.049

All dimensions in inches

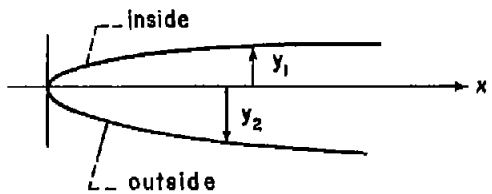

Typical cross section (A—A)

Figure 5.- Lip coordinates.

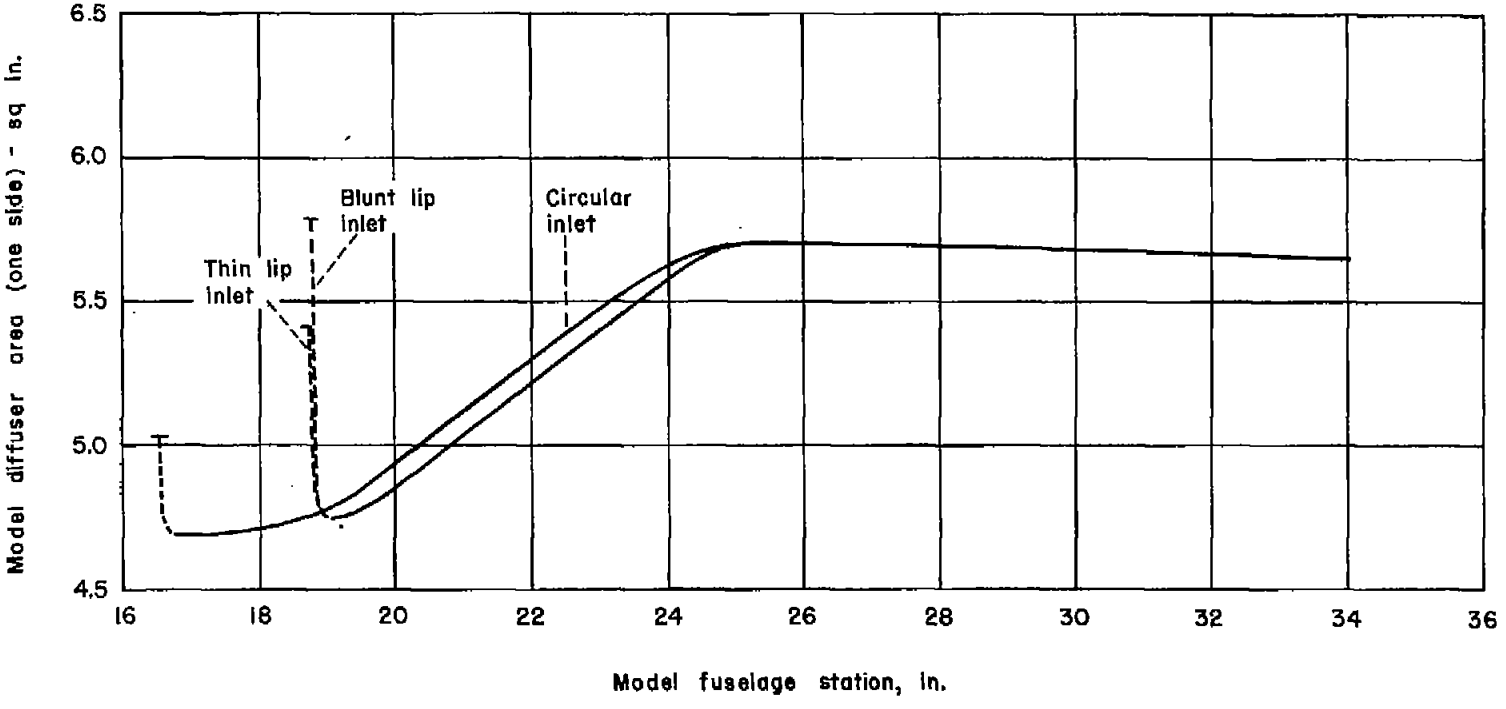

Figure 6.- Area variation in diffuser up to compressor station.

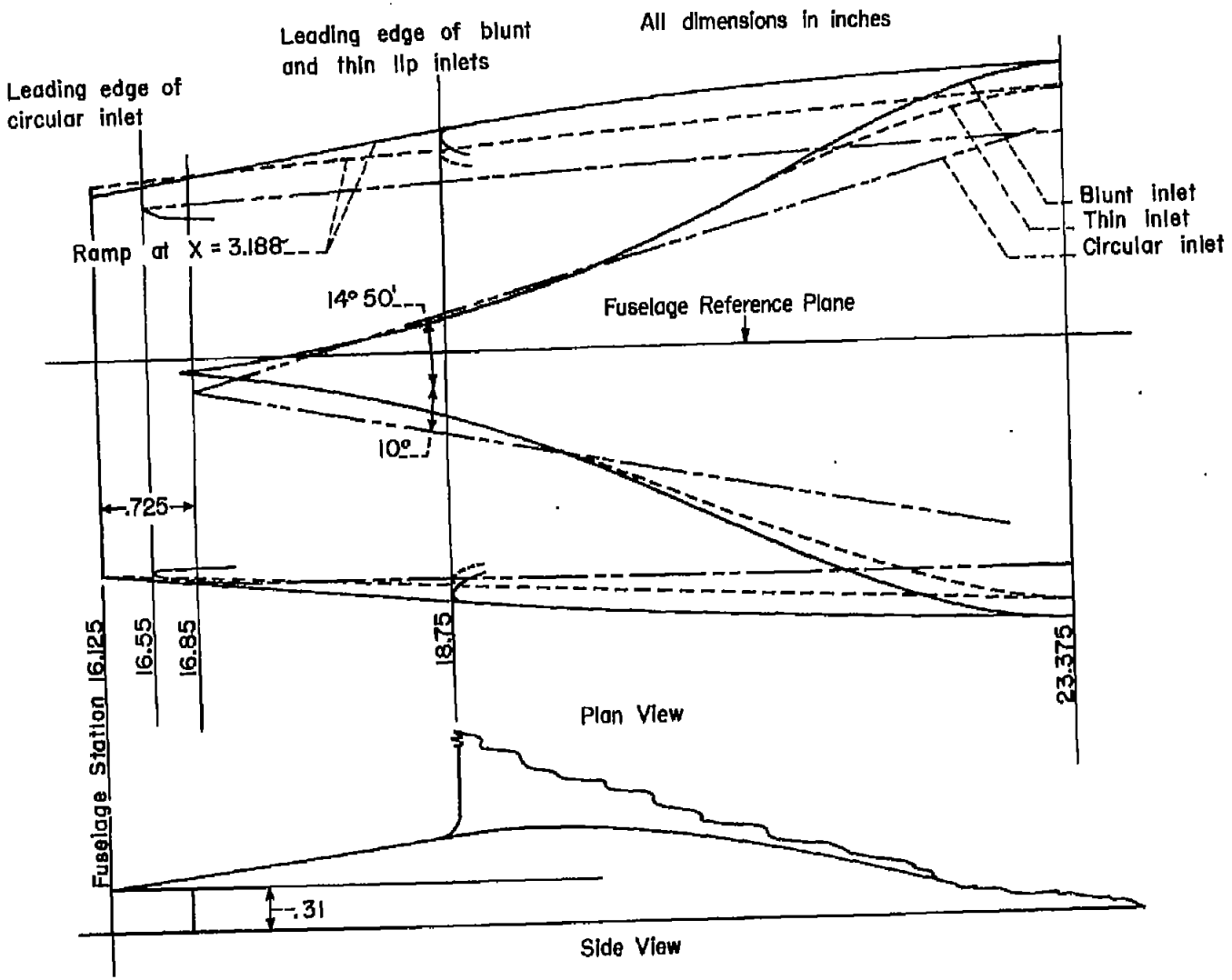

Figure 7.- A schematic comparison of the fuselage boundary-layer diverter wedges for the three inlets.

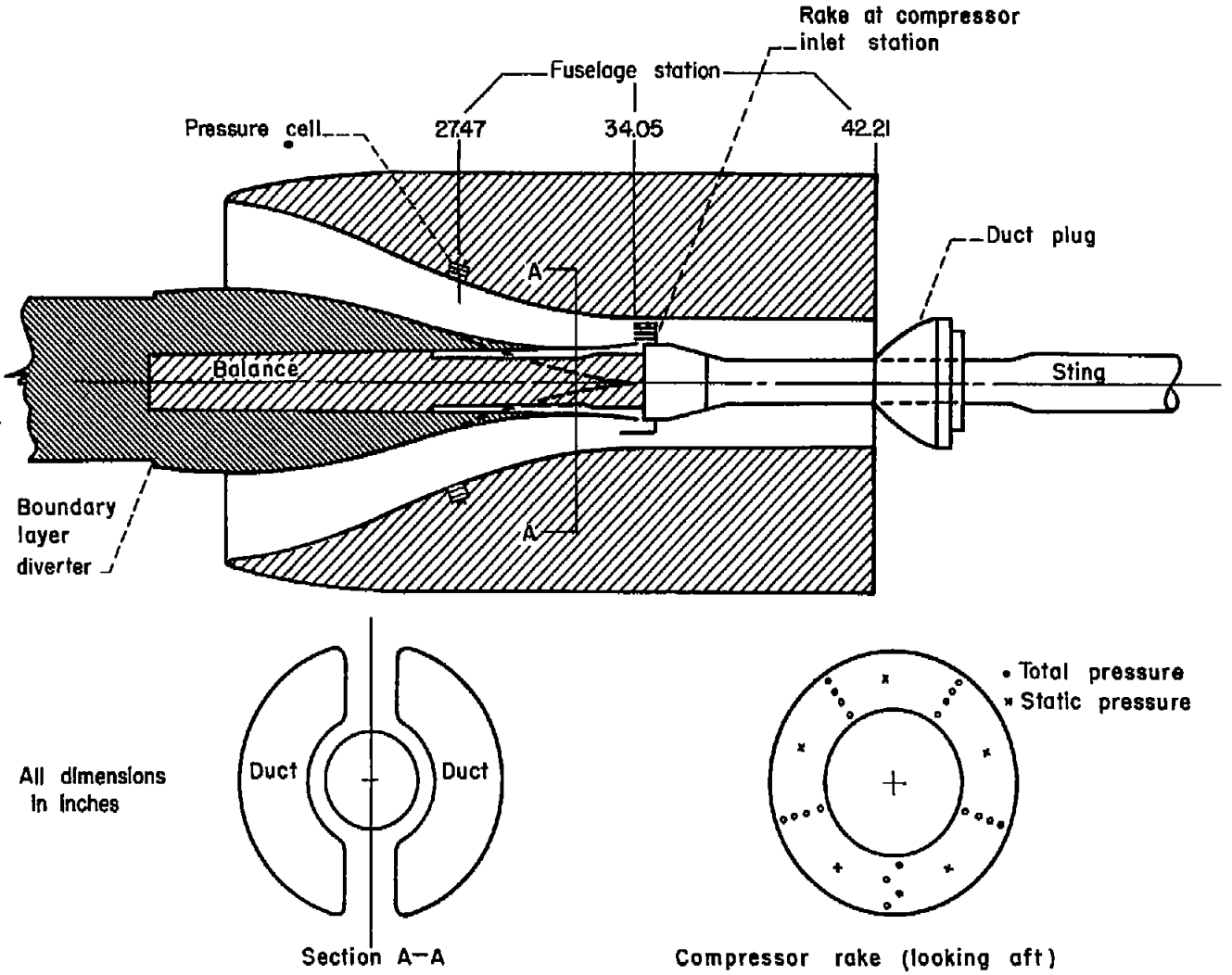

Figure 8.- Sketch of the air-induction model.

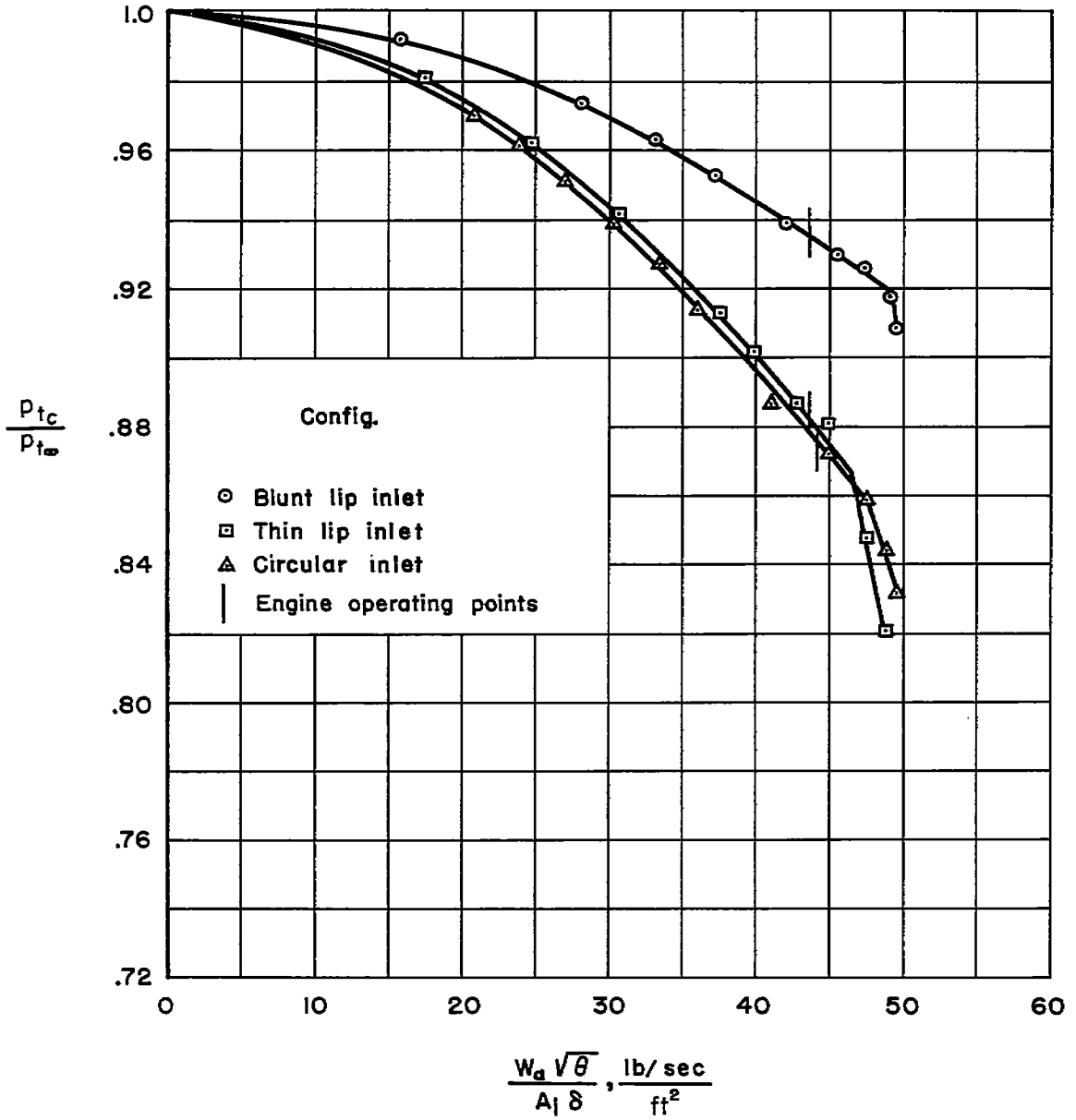

Figure 9.- The variation of pressure recovery with air-flow parameter for the take-off condition ($M_\infty = 0$).

[redacted]

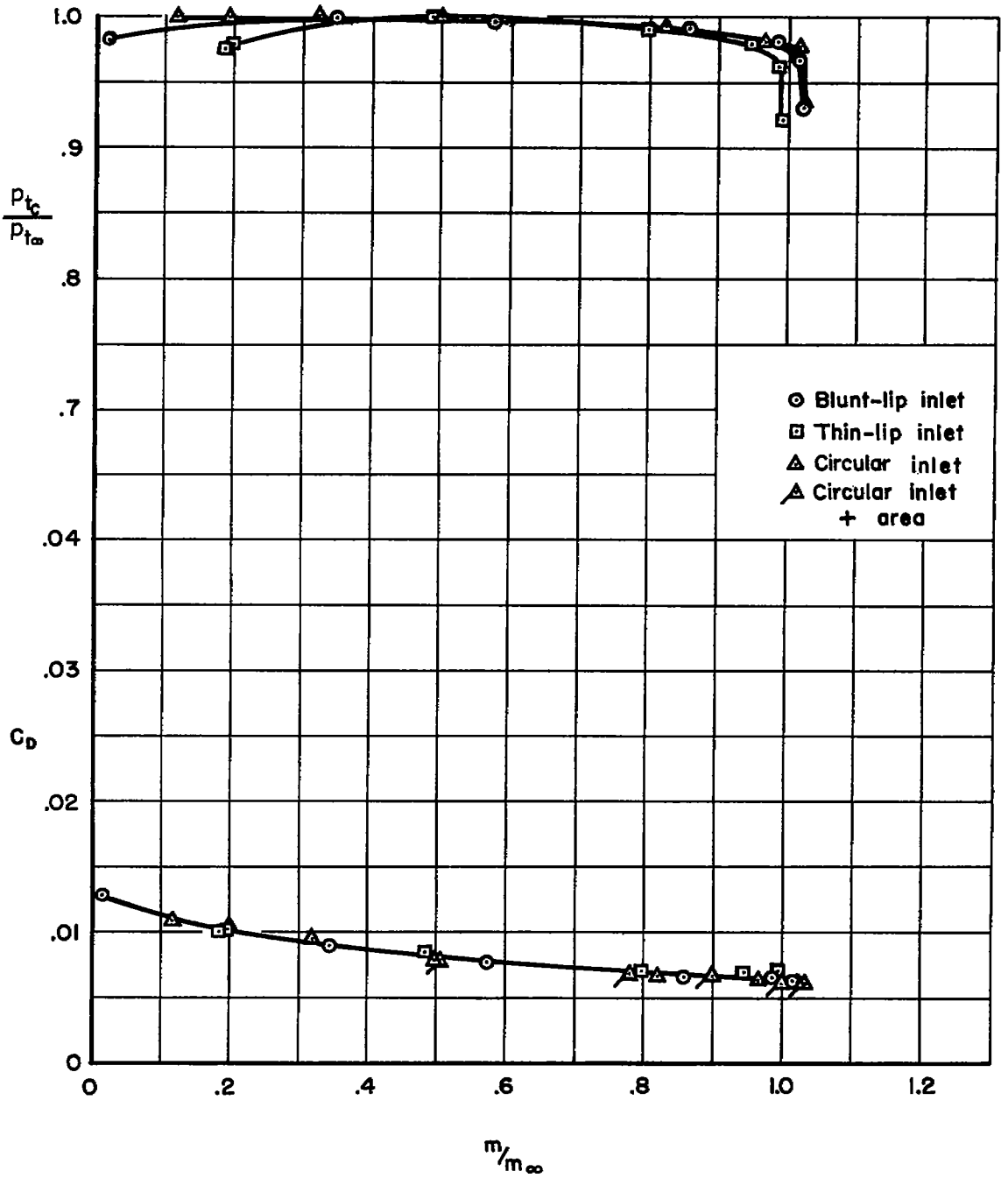

(a) $M_\infty = 0.9$

Figure 10.- Comparison of the performance characteristics of the blunt-lip, thin-lip, and circular inlets; $\alpha = 4.0°$.

[redacted]

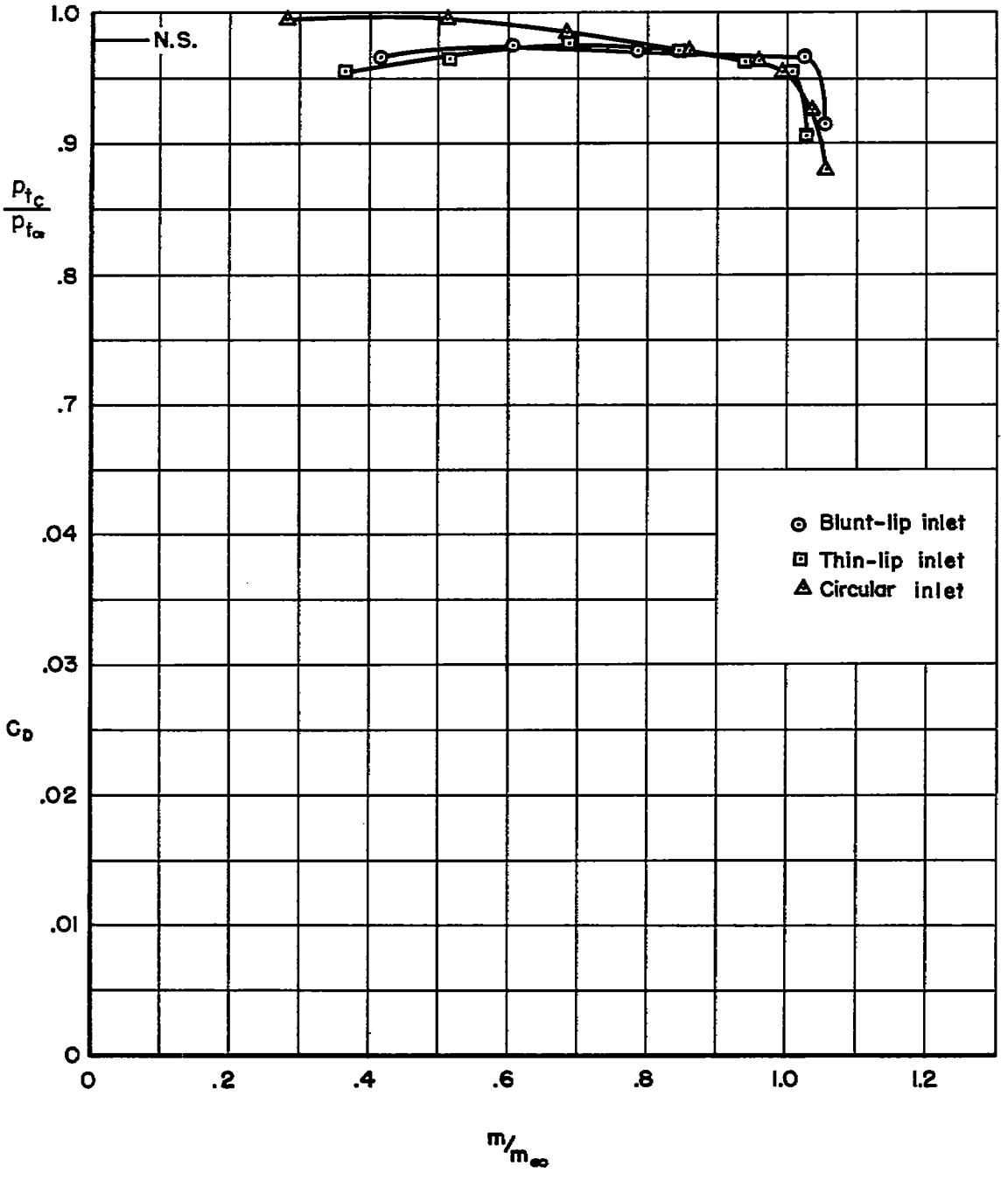

(b) $M_\infty = 1.3$

Figure 10.- Continued.

[redacted]

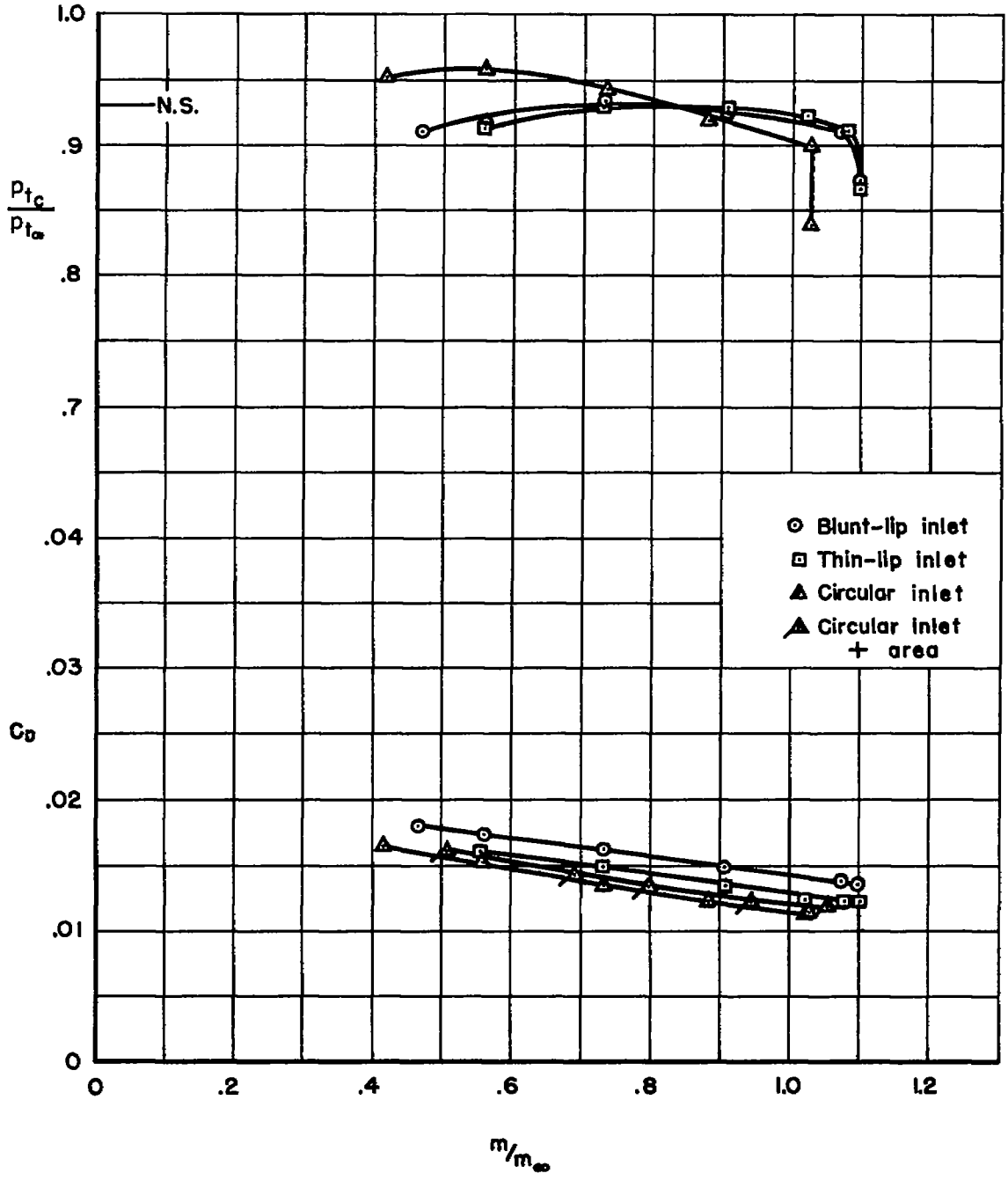

(c) $M_\infty = 1.5$

Figure 10.- Continued.

[redacted]

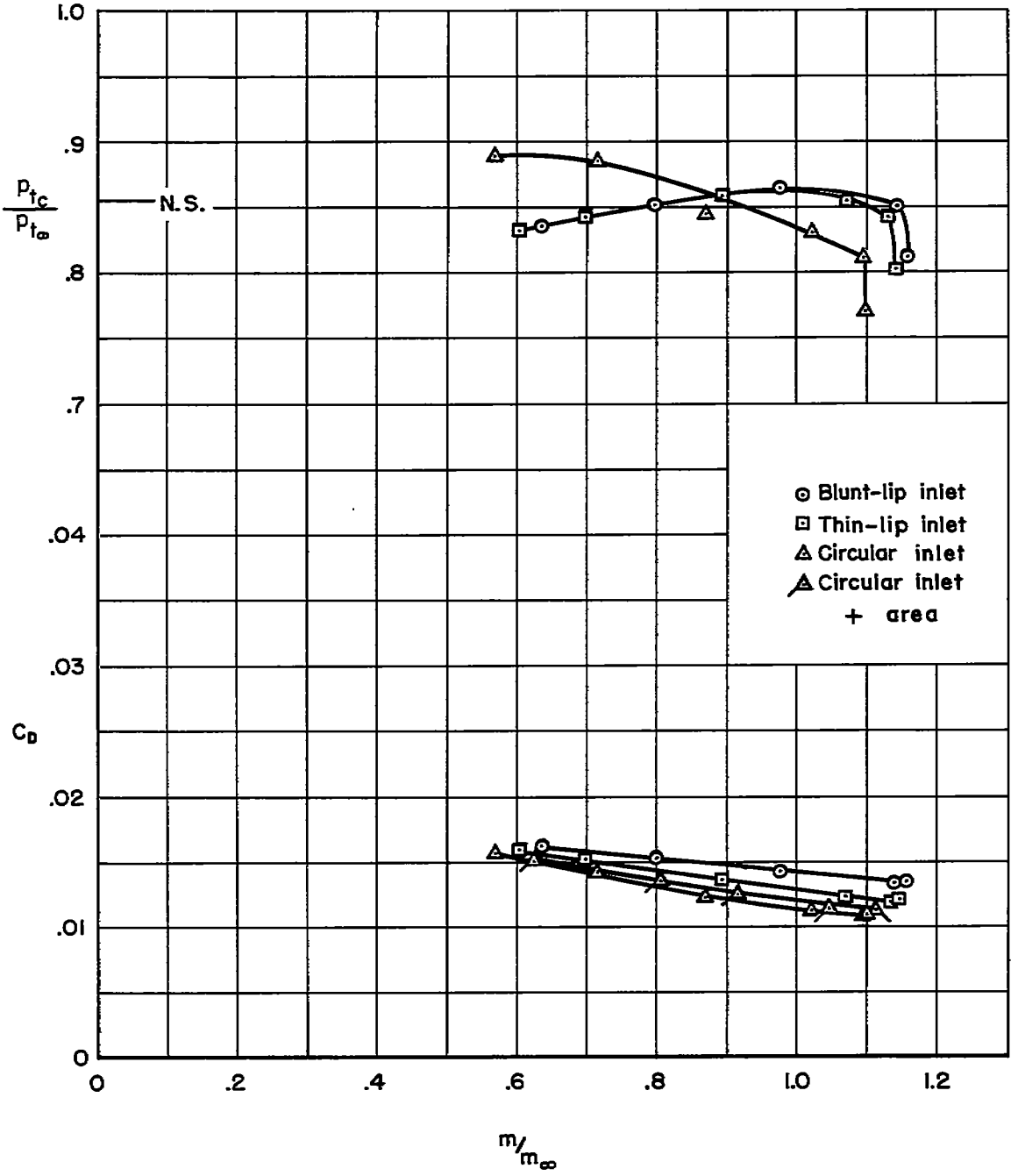

(d) $M_\infty = 1.7$

Figure 10.- Continued.

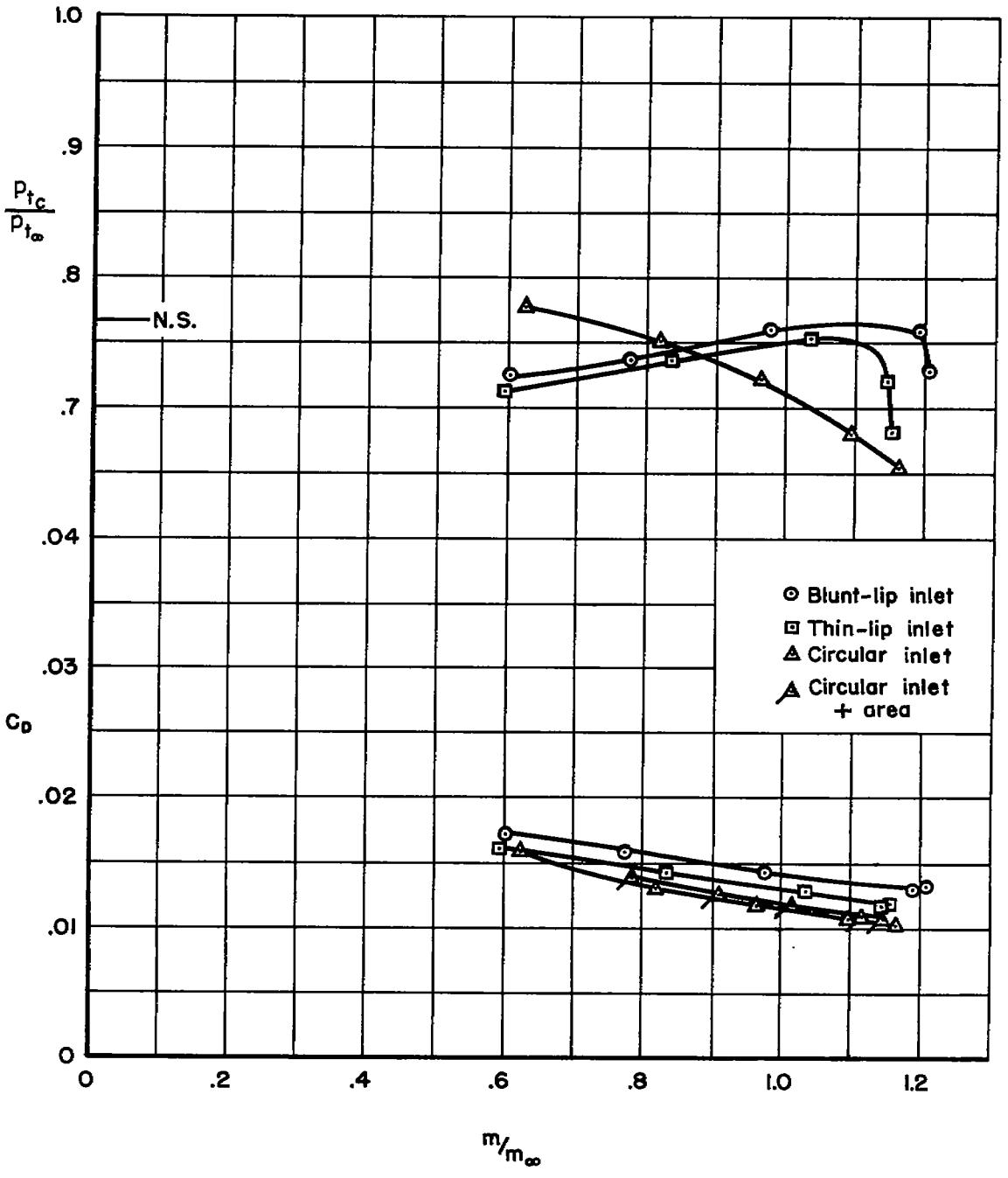

(e) $M_\infty = 1.9$

Figure 10.- Concluded.

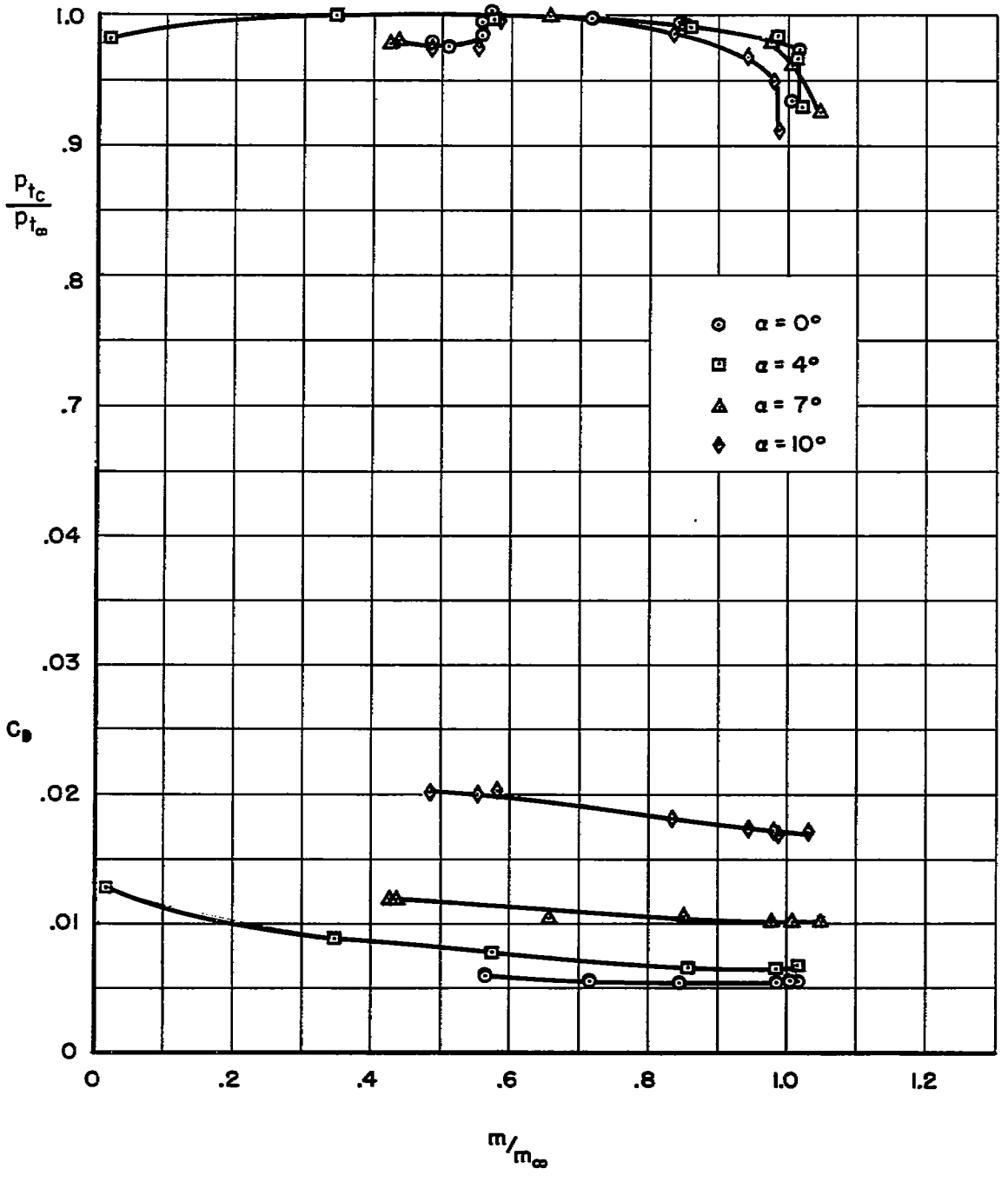

(a) $M_\infty = 0.9$

Figure 11.- The effect of angle of attack on the performance characteristics of the blunt-lip inlet.

[redacted]

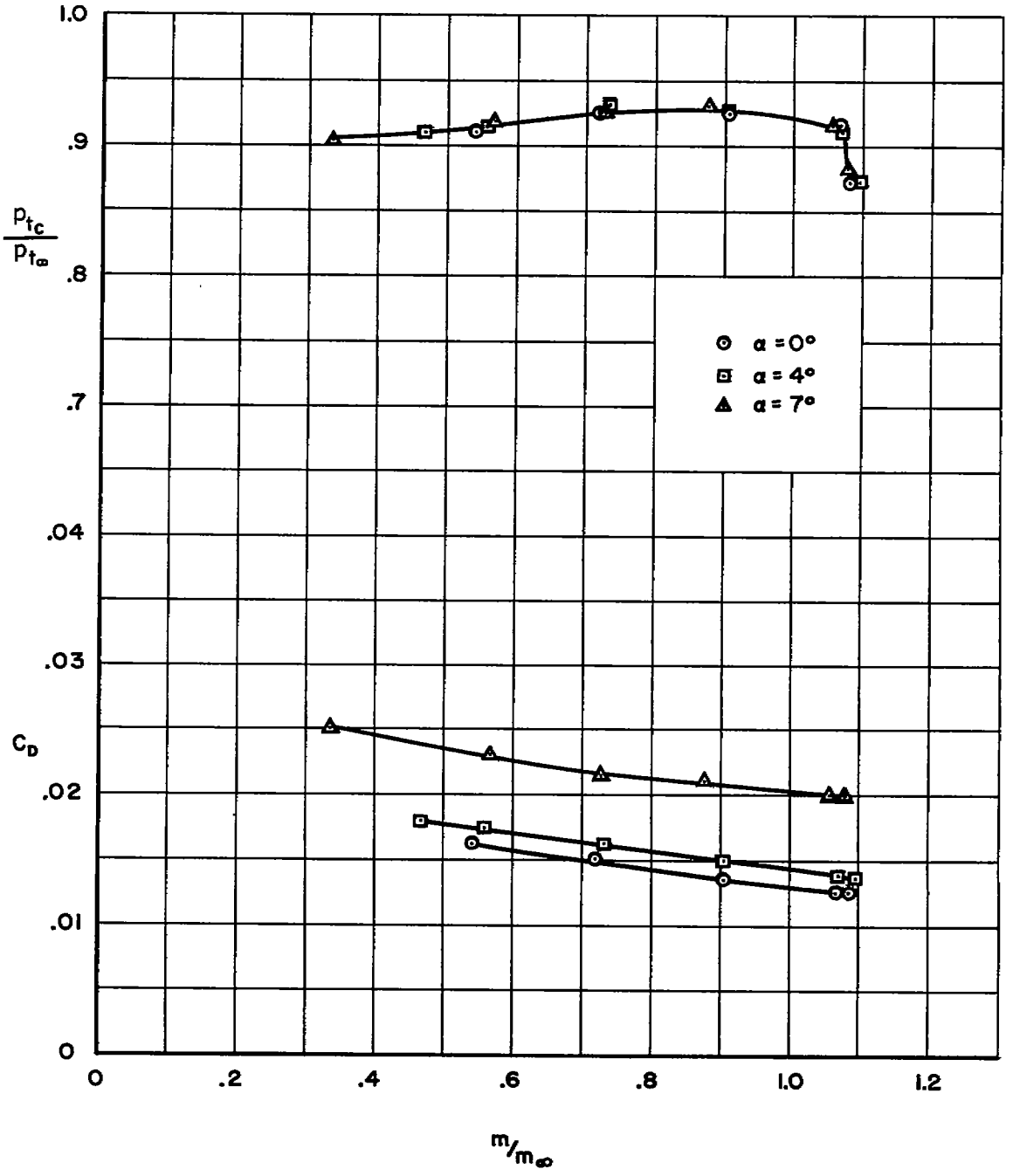

(b) $M_\infty = 1.5$

Figure 11.- Concluded.

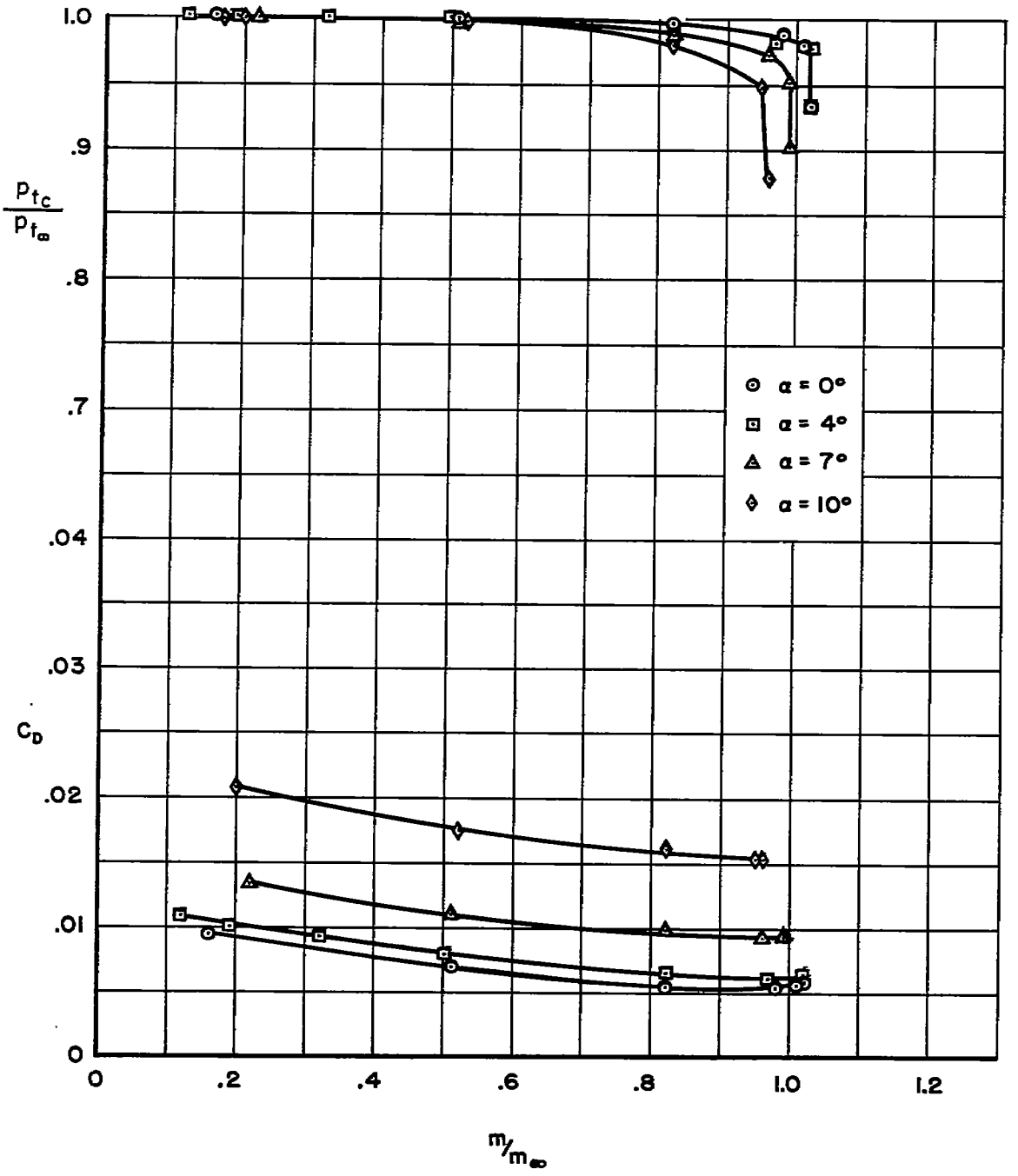

(a) $M_\infty = 0.9$

Figure 12.- The effect of angle of attack on the performance characteristics of the circular inlet.

[redacted]

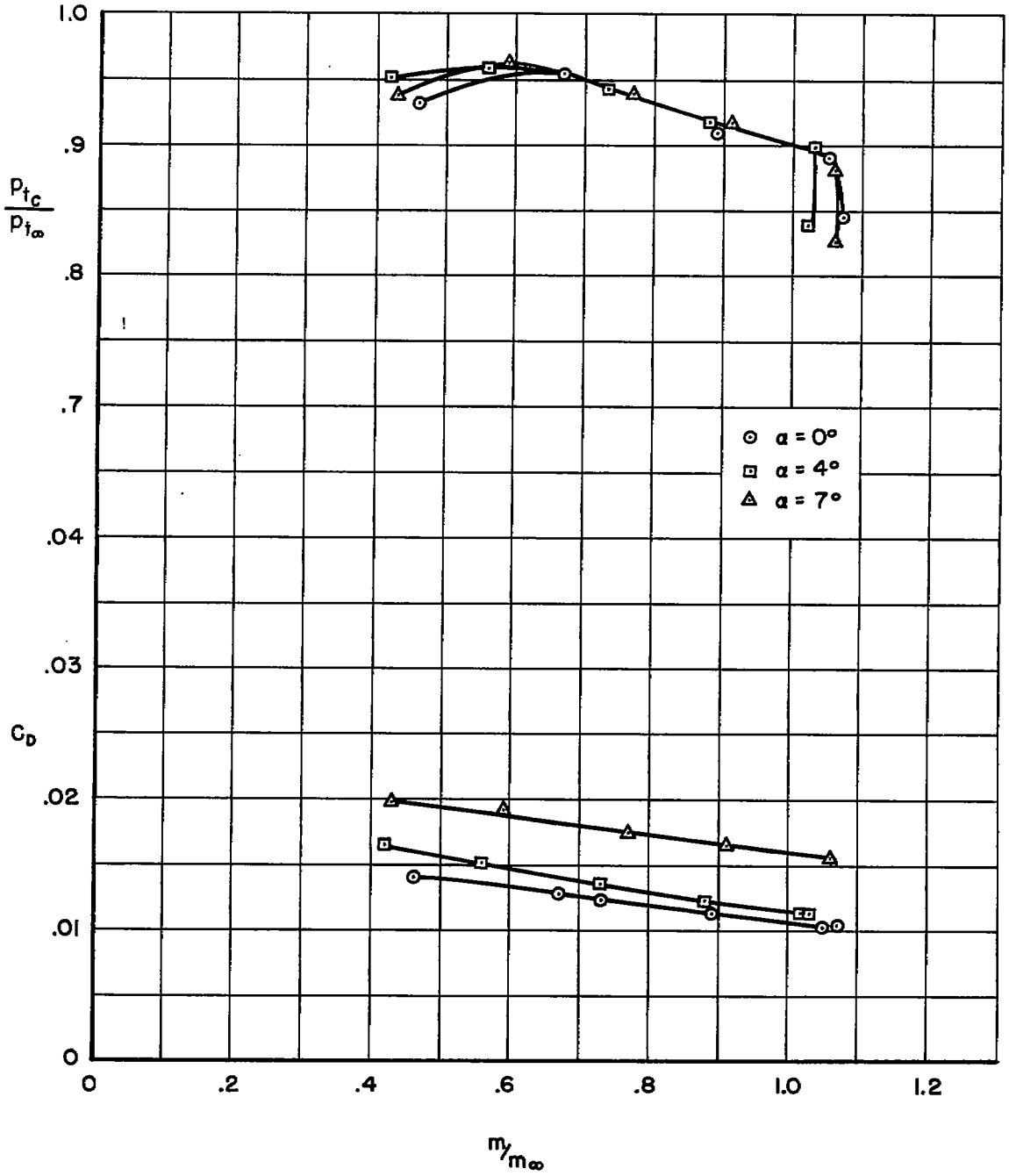

(b) $M_\infty = 1.5$

Figure 12.- Concluded.

[redacted]

$m/m_\infty \approx$ max

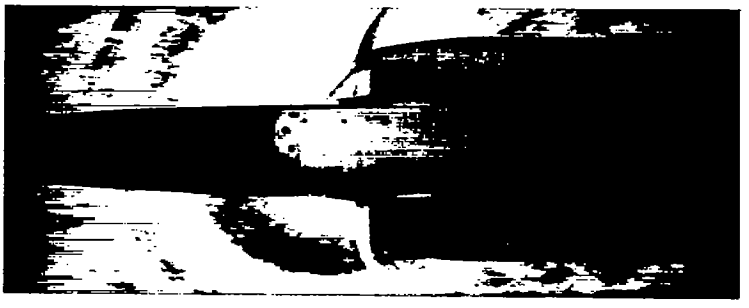

$m/m_\infty \approx 0.9$

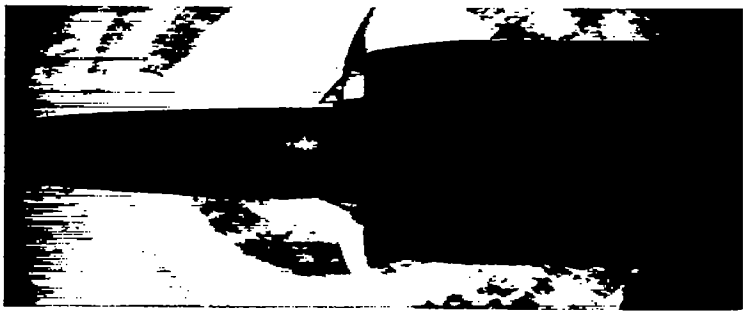

A-19256

$m/m_\infty \approx 0.6$

(a) Blunt-lip inlet.

Figure 13.- Schlieren photographs of air-induction model; $M_\infty = 1.5$, $\alpha = 4^\circ$.

[redacted]

$m/m_\infty \approx$ max

$m/m_\infty \approx 0.8$

A-19528

$m/m_\infty \approx 0.5$

(b) Thin-lip inlet.

Figure 13.- Continued.

$m/m_\infty \approx$ max

$m/m_\infty \approx 0.9$

A-19530

$m/m_\infty \approx 0.6$

(c) Circular inlet.

Figure 13.- Concluded.

[redacted]

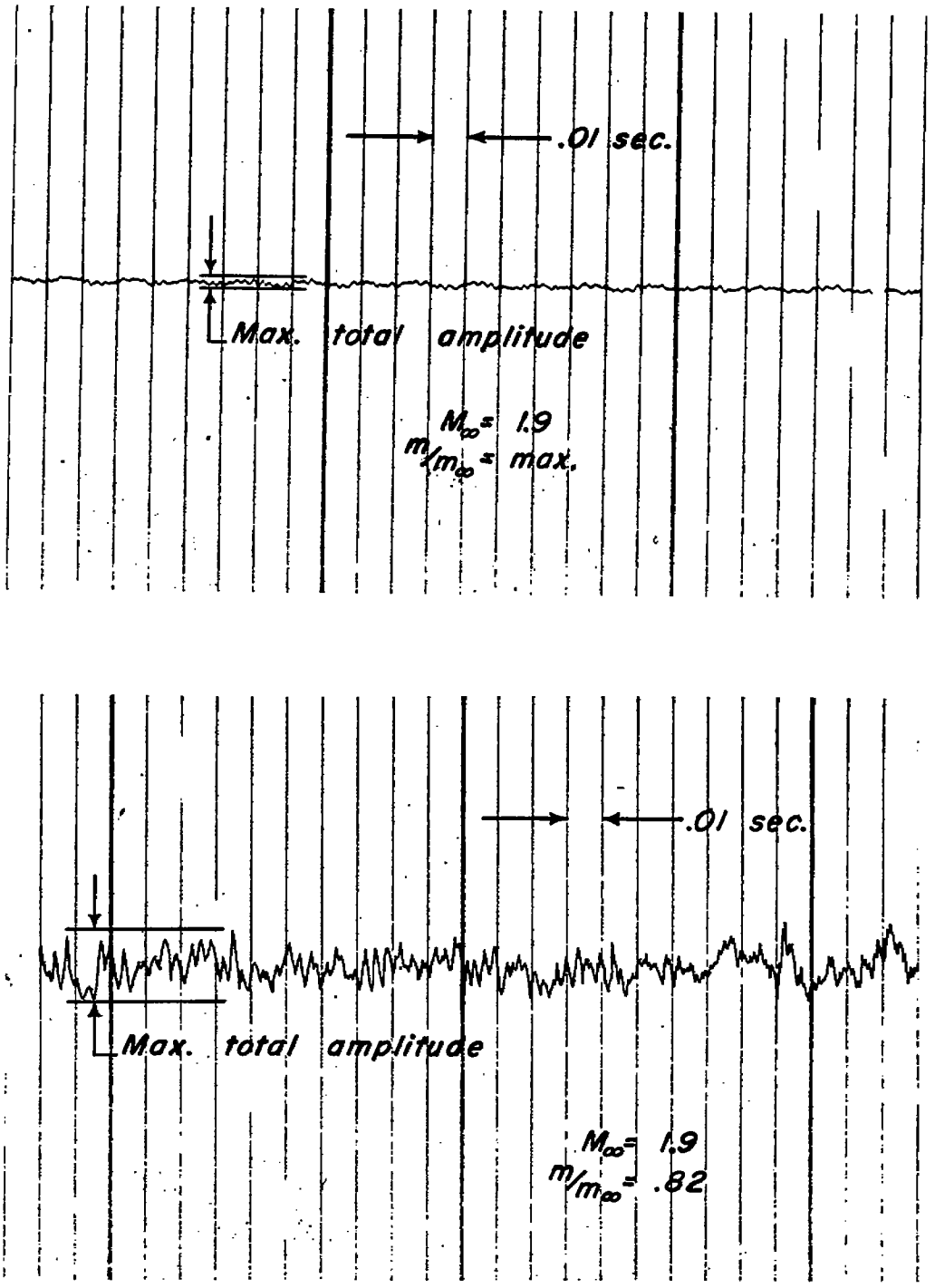

Figure 14.- Typical time-pressure records of the pressure pulsations, thin-lip inlet; $\alpha = 4^\circ$.

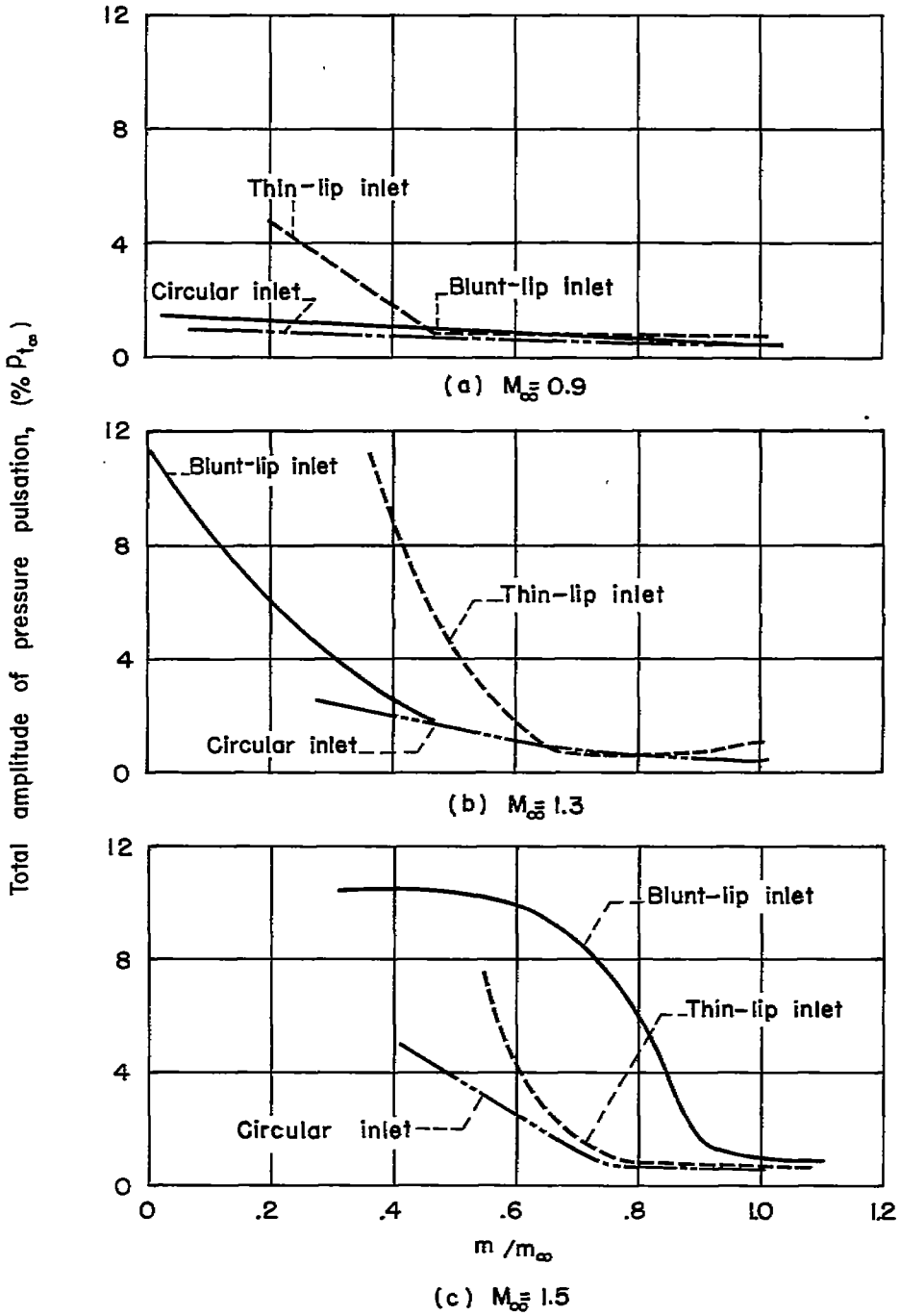

Figure 15.- Total amplitude of the pressure pulsations for three inlet configurations; $\alpha = 4^\circ$.

[redacted]

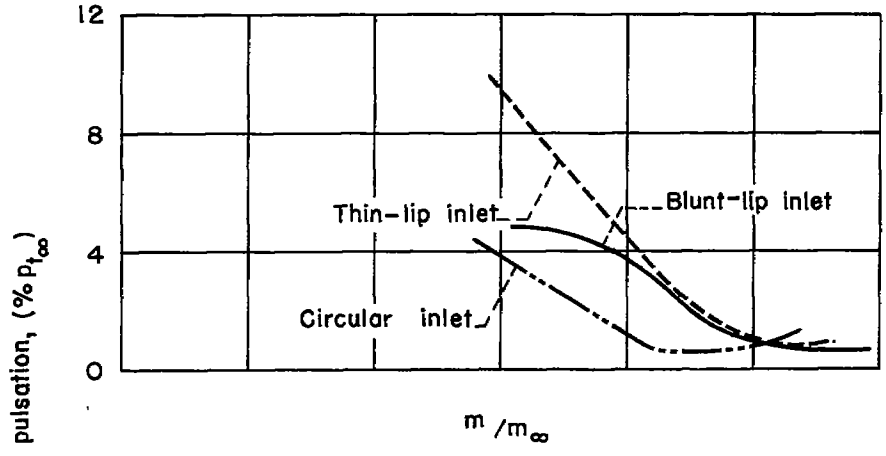

(d) $M_\infty = 1.7$

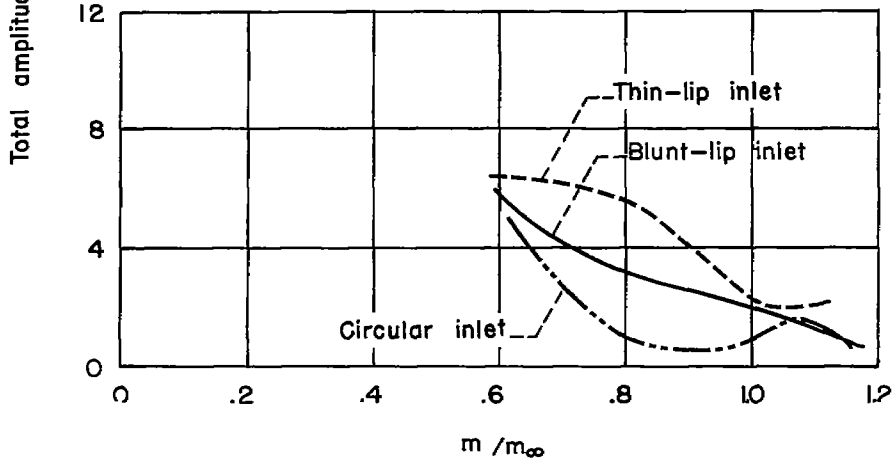

(e) $M_\infty = 1.9$

Figure 15.- Concluded.

[redacted]

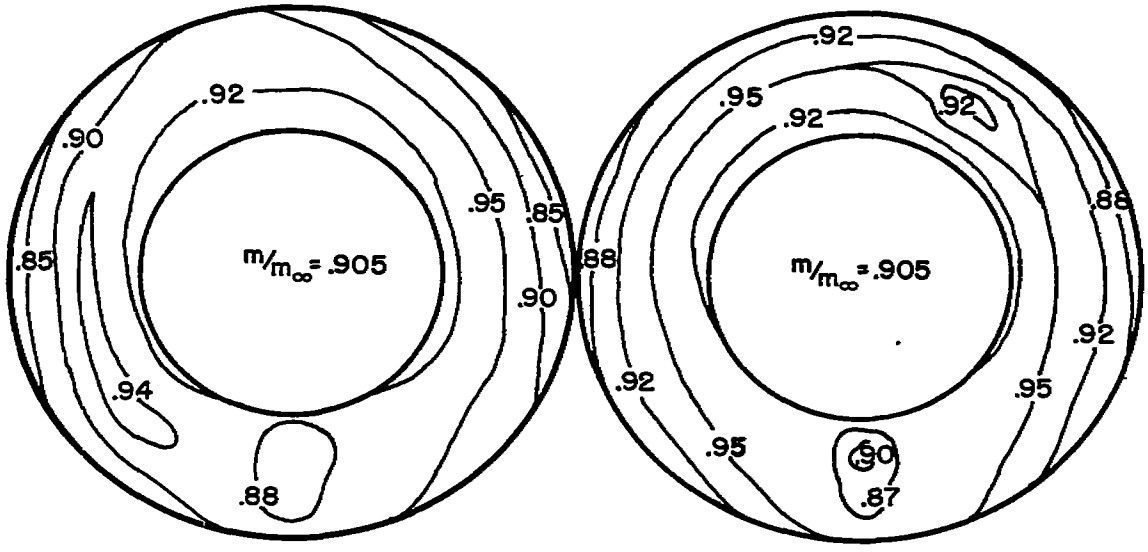

(a) Blunt-lip inlet.

(b) Thin-lip inlet.

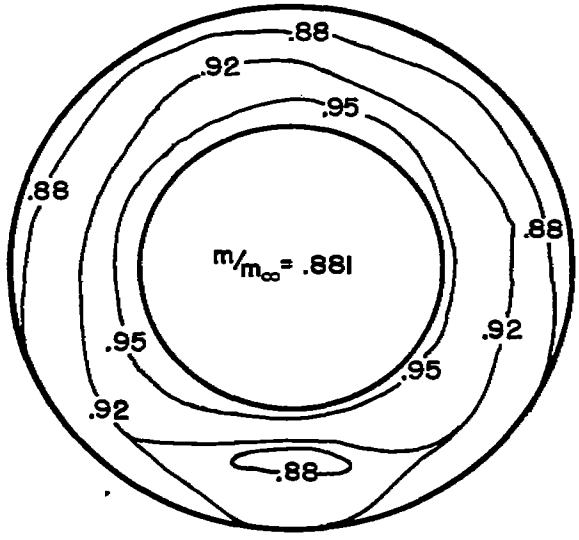

(c) Circular inlet.

Figure 16.- Typical total-pressure recovery contour maps for the blunt lip, thin-lip, and circular inlets; $M_\infty = 1.5$, $\alpha = 4.0^\circ$.

[redacted]

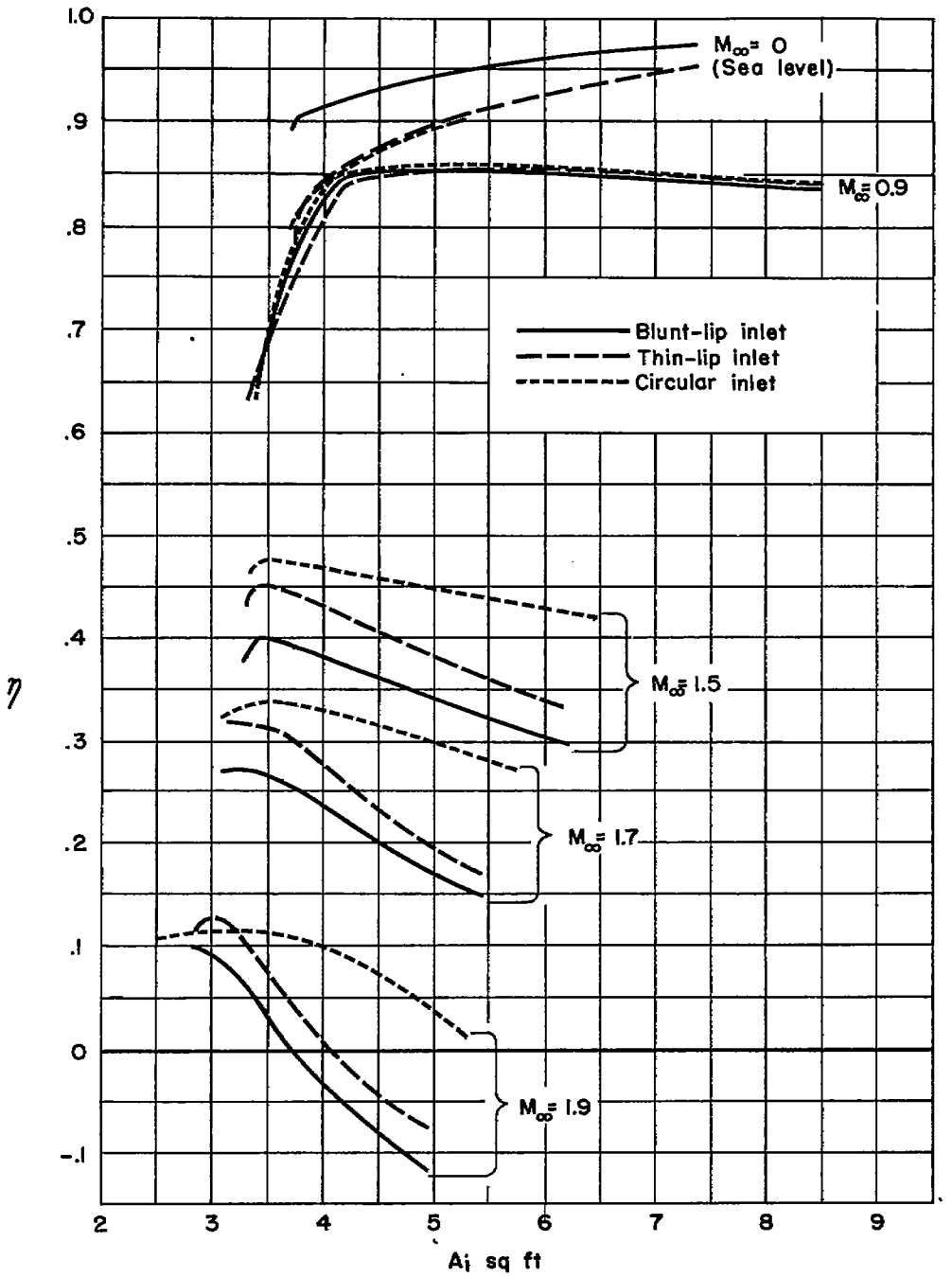

Figure 17.- Net-thrust parameter as a function of inlet area for the blunt-lip, thin lip, and circular inlets. (Altitude = 35,000 feet except as noted, JT-3C-20 engine.)

NACA - Langley Field, Va.